

KEY ISSUES REVIEW

Simulations of radiation pressure experiments narrow down the energy and momentum of light in matter

To cite this article: Max Bethune-Waddell and Kenneth J Chau 2015 *Rep. Prog. Phys.* **78** 122401

View the [article online](#) for updates and enhancements.

Related content

- [Non-conservative optical forces](#)
Sergey Sukhov and Aristide Dogariu
- [Tracing optical force fields within graded-index media](#)
Alireza Akbarzadeh, Mohammad Danesh, Cheng-Wei Qiu et al.
- [Roadmap on structured light](#)
Halina Rubinsztein-Dunlop, Andrew Forbes, M V Berry et al.

Recent citations

- [Verification of deforming polarized structure computation by using a closed-form solution](#)
B. Emek Abali and Felix A. Reich
- [Isolated detection of elastic waves driven by the momentum of light](#)
Tomaž et al
- [Electromagnetic stress tensor for an amorphous metamaterial medium](#)
Neng Wang et al



IOP | ebooks™

Bringing you innovative digital publishing with leading voices to create your essential collection of books in STEM research.

Start exploring the collection - download the first chapter of every title for free.

Key issues review

Simulations of radiation pressure experiments narrow down the energy and momentum of light in matter

Max Bethune-Waddell and Kenneth J Chau

School of Engineering, The University of British Columbia, Kelowna, Canada

E-mail: kenneth.chau@ubc.ca

Received 22 April 2014, revised 3 September 2015

Accepted for publication 8 September 2015

Published 28 October 2015



Abstract

Consensus on a single electrodynamic theory has yet to be reached. Discord was seeded over a century ago when Abraham and Minkowski proposed different forms of electromagnetic momentum density and has since expanded in scope with the gradual introduction of other forms of momentum and force densities. Although degenerate sets of electrodynamic postulates can be fashioned to comply with global energy and momentum conservation, hope remains to isolate a single theory based on detailed comparison between force density predictions and radiation pressure experiments. This comparison is two-fold challenging because there are just a handful of quantitative radiation pressure measurements over the past century and the solutions developed from different postulates, which consist of approximate expressions and inferential deductions, are scattered throughout the literature. For these reasons, it is appropriate to conduct a consolidated and comprehensive re-analysis of past experiments under the assumption that the momentum and energy of light in matter are degenerate. We create a combined electrodynamic/fluid dynamic simulation testbed that uses five historically significant sets of electrodynamic postulates, including those by Abraham and Minkowski, to model radiation pressure under diverse configurations with minimal assumptions. This leads to new interpretations of landmark investigations of light momentum, including the Balazs thought experiment, the Jones–Richards and Jones–Leslie measurements of radiation pressure on submerged mirrors, observations of laser-deformed fluid surfaces, and experiments on optical trapping and tractor beaming of dielectric particles. We discuss the merits and demerits of each set of postulates when compared to available experimental evidence and fundamental conservation laws. Of the five sets of postulates, the Abraham and Einstein–Laub postulates provide the greatest consistency with observations and the most physically plausible descriptions of electrodynamic interactions. Force density predictions made by these two postulates are unique under many conditions and their experimental isolation is potentially within reach.

Keywords: radiation pressure, electromagnetic momentum density, Abraham–Minkowski controversy, Lorentz force law, electrodynamics, laser-induced fluid deformation, optical tweezers

(Some figures may appear in colour only in the online journal)

1. Introduction

Radiation pressure was first predicted by Maxwell as a natural consequence of the energy and momentum content of electromagnetic fields [1]. In the early 1900s, measurements of radiation pressure on mirrors in vacuum [2–4] provided visceral evidence of momentum conversion between electromagnetic and mechanical forms. Shortly after, competing theories were introduced by Minkowski [5] and Abraham [6] to describe the momentum density of electromagnetic waves in terms of classical field quantities, the keystone of a complete electrodynamic theory of light-matter interaction. Minkowski proposed a form given by $\vec{D} \times \vec{B}$, with \vec{D} representing the displacement field and \vec{B} the magnetic flux density, and Abraham introduced a form given by $(\vec{E} \times \vec{H})/c^2$, with \vec{E} representing the electric field, \vec{H} the magnetic field, and c the speed of light. Although identical in vacuum, the Abraham and Minkowski forms give divergent predictions of the electromagnetic momentum density in matter. If we consider an electromagnetic wave entering a dielectric medium of refractive index n from free space, the Minkowski form predicts an electromagnetic momentum increase proportional to n , whereas the Abraham form predicts an electromagnetic momentum decrease proportional to $1/n$. Dichotomy between the theories of Abraham or Minkowski became known as the Abraham–Minkowski controversy. This debate has grown in scope over the past century to include alternative electrodynamics theories [7–11] and has lead to basic questions about the nature of electromagnetic power flow, the distribution of electromagnetic force, and the implications of observable pressure imparted by radiation to matter.

At different points in time over the past century, compelling claims have been made in support of the Minkowski or Abraham forms of electromagnetic momentum. Experimental measurements of radiation pressure on submerged mirrors [12, 13], fluid interfaces [14–19], semiconductors carriers [20–22], and dilute atom gases [23] have consistently revealed a refractive-index proportionality most commonly interpreted to support the Minkowski momentum density [24–27]. The Minkowski form of momentum can also be derived by considering the Doppler-shifted momentum imparted by a photon to an absorber [27–32]. On the other hand, convincing theoretical arguments have been developed in support of the Abraham momentum density. When used with a canonical form of the Poynting vector $\vec{E} \times \vec{H}$ [33], the Abraham momentum density forms an energy-momentum tensor that is diagonally symmetric and therefore, consistent with angular momentum conservation [34–36]. Moreover, Balazs [37] put forward an extension of the Einstein photon-in-box thought experiment [38] to show that only the Abraham momentum preserves linear center-of-mass translation in a closed system consisting of a rigid, reflection-less dielectric block and an electromagnetic pulse. Strong evidence for the Minkowski and Abraham momentum densities has led to an acceptance of the potential correctness of both [25, 26, 39, 40] and a heuristic approach to their application: the Minkowski or ‘wave’ momentum can be used to predict radiation pressure phenomena whereas the Abraham or ‘kinetic’ momentum can be used to predict center-of-mass translations [29, 41–45].

In the 1960s, Penfield and Haus [10] showed that multiple electrodynamic formulations can describe the evolution of energy and momentum in a closed system in a manner consistent with global energy and momentum conservation. The starting point is a general framework in which a closed system is decomposed into a set of coupled sub-systems. For example, a closed system containing ponderable matter and electromagnetic fields could be broken down into a kinetic sub-system describing the mechanical motion of matter, a thermodynamic sub-system describing the energy flow in matter, and an electrodynamic sub-system describing the momentum and energy stored in the fields. Each sub-system is modelled using energy and momentum continuity equations, which take on the generic forms

$$\nabla \cdot \vec{S} + \frac{\partial}{\partial t} W = -\phi \quad (1)$$

and

$$\nabla \cdot \vec{T} + \frac{\partial}{\partial t} \vec{G} = -\vec{f}, \quad (2)$$

respectively, where \vec{T} is the stress tensor, \vec{G} the electromagnetic momentum density, \vec{f} the force density, \vec{S} the energy flux density, W the energy density, and ϕ the power density. In a closed system, the continuity equations of the various sub-systems, indexed by the variable l , are coupled so that

$$\Sigma \phi_l = 0 \quad (3)$$

and

$$\Sigma \vec{f}_l = 0, \quad (4)$$

which means that energy and momentum simply move between systems and enables the entire model to be validated against global energy and momentum conservation laws.

Energy, momentum, power, stress, and force in the electrodynamic sub-system are defined in terms of \vec{E} , \vec{D} , \vec{H} , and \vec{B} and together constitute a set of electrodynamic postulates. There are many ways to formulate the postulates to satisfy the continuity equations. Empirical validation of an entire set of postulates is difficult because fields in matter cannot be directly measured. Attempts were made in the mid-1900s [12–14] to test different postulates of momentum by measuring radiation pressure on illuminated objects, but consistent interpretation of these experiments has been elusive. Radiation pressure on submerged mirrors [13], for example, has been explained in terms of the Minkowski momentum [24–27], the Abraham momentum [46], the arithmetic mean of the two [47–50], or a canonical momentum of quantum mechanical origins [51]. To reconcile the disparate literature, two mutually-exclusive hypotheses have emerged: either the definition of momentum is totally arbitrary and there are many simultaneously valid electrodynamic theories [40, 45, 52, 53] or there is a single theory that uniquely predicts observable phenomena but has thus far escaped experimental detection [54]. We argue the latter.

Although various electrodynamic formulations can be consistent with conservation laws, their predicted observables can differ depending on how momentum and energy are parsed

between electromagnetic and mechanical forms. As a result, different sets of self-consistent postulates can yield different predictions of force density [24, 55–58], suggesting that they are experimentally distinguishable and only one should best approximate natural behaviour. With this in mind, we start with five historically significant sets of electrodynamic postulates and perform a consolidated analysis of past radiation pressure experiments to find out which, if any, achieves total consistency with observations to date. We re-visit landmark investigations of light momentum including arguments based on center-of-mass translation, radiation pressure measurements on fluid-submerged mirrors, observations of radiation-induced deformation of fluid interfaces, and manipulation of small dielectric particles by laser beams. Although all five postulates can be made consistent with conservation laws, the postulates proposed by Abraham and Einstein–Laub are the most physically plausible, as they offer generally satisfactory accounts of radiation pressure experiments across the board while maintaining consistency with other fundamental principles. We show that the Abraham and Einstein–Laub postulates can potentially be distinguished in configurations within contemporary experimental techniques, providing a means for empirical validation of a single electrodynamic theory.

2. Theory

Following the approach of Penfield and Haus [10], we consider a thermodynamically closed system containing an electrodynamic sub-system supplying energy and momentum in the form of electromagnetic fields and a kinetic sub-system composed of the material body acted upon by the fields. The overall system is bound by two fundamental and incontrovertible laws: the total energy and momentum appearing in both electromagnetic and mechanical forms must be globally conserved, and mass and energy are equivalent within a factor c^2 [59, 60].

2.1. Electrodynamic sub-system

The energy and momentum of electromagnetic fields in matter are described by classical field theory. Such a treatment implicitly ignores microscopic fluctuations of energy and momentum in a medium due to quantum-mechanical photon-atom interactions, allowing the medium to be treated as a continuum with sharp, well-defined boundaries. Maxwell's equations, given by

$$\nabla \times \vec{E} = -\frac{\partial}{\partial t} \vec{B}, \quad (5)$$

$$\nabla \times \vec{H} = \frac{\partial}{\partial t} \vec{D} + \vec{J}, \quad (6)$$

$$\nabla \cdot \vec{B} = 0, \quad (7)$$

and

$$\nabla \cdot \vec{D} = \rho_e, \quad (8)$$

describe the spatial and temporal evolutions of field quantities—electric field \vec{E} , magnetic field \vec{H} , displacement field \vec{D} , and magnetic flux density \vec{B} —and source quantities—current density \vec{J} and charge density ρ_e . In matter, the polarization density is given by $\vec{P} = \vec{D} - \epsilon_0 \vec{E}$ and the magnetization density is given by $\vec{M} = \vec{B} - \mu_0 \vec{H}$, where ϵ_0 is the free-space permittivity and μ_0 is the free-space permeability. Both field and source quantities can exist in vacuum or matter and are piecewise smooth everywhere. There are different conventions for attaching physical significance to the field quantities and distinguishing their behavior in vacuum and matter. The Minkowski formulation places all four field variables, \vec{E} , \vec{H} , \vec{D} , and \vec{B} , on equal footing and makes no formal distinction between fields in vacuum and matter. The Chu and Amperian formulations, on the other hand, identify \vec{E} as the vacuum electric field and either \vec{H} or \vec{B} , respectively, as the vacuum magnetic field. Differences between the Chu and Amperian formulations arise because magnetization is modelled by the former as magnetic charge density and the latter as magnetic current loops. Although intuitive, a description of magnetization in terms of current loops must also invoke the notion that the loop possesses intrinsic hidden momentum and energy [10, 57, 61, 62].

Energy and momentum continuity within the electrodynamic sub-system are respectively described by

$$\nabla \cdot \vec{S}_e + \frac{\partial}{\partial t} W_e = -\phi_e \quad (9)$$

and

$$\nabla \cdot \vec{T}_e + \frac{\partial}{\partial t} \vec{G}_e = -\vec{f}_e, \quad (10)$$

where densities of power, energy, stress, and momentum are generically encapsulated, respectively, in the variables \vec{S}_e , W_e , \vec{T}_e , and \vec{G}_e . The terms ϕ_e and \vec{f}_e describe the respective rate of energy and momentum transfer from the fields to matter, which are not directly measurable but can be inferred from the response of the material body on which the fields act. Note that Maxwell's equations can be manipulated in several ways to take the form of the energy and momentum continuity equations. The classical derivation of the Poynting theorem, for example, is based on re-casting Maxwell's equations in the form of energy continuity [8, 33, 63, 64]. The Poynting vector has been defined most commonly as $\vec{E} \times \vec{H}$ but, if \vec{B} is viewed as the fundamental magnetic field, has also been defined as $\vec{E} \times \vec{B}/\mu_0$ [65, 66]. These two forms have differing consequences in magnetic media, but neither one has been proven to be more correct than the other.

2.2. Kinetic sub-system

We adopt classical Newtonian dynamics to describe the energy and momentum associated with the motion of macroscopic material bodies. Such an approach assumes that a medium moves at non-relativistic speeds and that quantum mechanical interactions between atoms of the medium can be ignored. Energy and momentum within the kinetic sub-system are respectively described by

Table 1. Momentum density, stress tensor, and power flux corresponding to the Minkowski, Abraham, Einstein–Laub, Amperian, and Chu formulations of electrodynamics.

Form	Momentum density	Power flux	Stress tensor
Minkowski ^a	$\vec{D} \times \vec{B}$	$\vec{E} \times \vec{H}$	$(\vec{D} \cdot \vec{E} + \vec{B} \cdot \vec{H})\vec{I}/2 - \vec{D}\vec{E} - \vec{B}\vec{H}$
Abraham	$\vec{E} \times \vec{H}/c^2$	$\vec{E} \times \vec{H}$	$[(\vec{D} \cdot \vec{E} + \vec{B} \cdot \vec{H})\vec{I} - \vec{D}\vec{E} - \vec{B}\vec{H} - \vec{E}\vec{D} - \vec{H}\vec{B}]/2$
Einstein–Laub	$\vec{E} \times \vec{H}/c^2$	$\vec{E} \times \vec{H}$	$(\epsilon_0 \vec{E}^2 + \mu_0 \vec{H}^2)\vec{I}/2 - \vec{D}\vec{E} - \vec{B}\vec{H}$
Amperian	$\epsilon_0 \vec{E} \times \vec{B}$	$\vec{E} \times \vec{B}/\mu_0$	$(\epsilon_0 \vec{E}^2 + \mu_0^{-1} \vec{B}^2)\vec{I}/2 - \epsilon_0 \vec{E} \vec{E} - \mu_0^{-1} \vec{B} \vec{B}$
Chu	$\vec{E} \times \vec{H}/c^2$	$\vec{E} \times \vec{H}$	$(\epsilon_0 \vec{E}^2 + \mu_0 \vec{H}^2)\vec{I}/2 - \epsilon_0 \vec{E} \vec{E} - \mu_0 \vec{H} \vec{H}$

^a The Minkowski energy-momentum tensor is presented in its classical asymmetric form [5, 77]. We will also consider a symmetric form in which the Minkowski momentum density is paired with a definition of power flux $c^2 \vec{D} \times \vec{B}$. This power flux definition is different from the canonical Poynting vector, but achieves a symmetric energy-momentum tensor that is consistent with equation (15).

$$\nabla \cdot \left(\frac{1}{2} \rho v^2 \vec{v} \right) + \frac{\partial}{\partial t} \left(\frac{1}{2} \rho v^2 \right) = \phi_m \quad (11)$$

and

$$\nabla \cdot (\rho \vec{v} \vec{v}) + \frac{\partial}{\partial t} \rho \vec{v} = \vec{f}_m, \quad (12)$$

where ρ is the mass density, \vec{v} is the local velocity, and the terms ϕ_m and \vec{f}_m describe the respective rates of energy and momentum transfer to matter. The kinetic energy of the sub-system can be ignored by noting that the mass density obeys the continuity relation

$$\nabla \cdot (\rho \vec{v}) + \frac{\partial}{\partial t} \rho = 0. \quad (13)$$

Hence, to first order of velocity, the first two terms of equation (11) cancel and $\phi_m = 0$. The same result can be achieved under the quasi-stationary approximation, which treats the kinetic sub-system in the limits $\rho \rightarrow \infty$ and $\vec{v} \rightarrow 0$ such that the kinetic energy goes to zero while the momentum remains finite [34]. This requires that the electromagnetic fields cause negligible displacement of the material and that the rest mass energy of the material is substantially larger than the electromagnetic energy of the fields. For all practical purposes, both assumptions are valid.

We will consider the application of electromagnetic force density to a material system which is generally allowed to be viscous, deformable, and multi-component. We do, however, restrict the material to be incompressible, which is in strict violation of relativity but gives reasonable first-order estimates so long as the material moves at non-relativistic speeds. The rate of momentum transfer to the material system is modelled using the incompressible Navier–Stokes equation

$$\vec{f}_m = \rho \vec{g} + \vec{f}_e + \vec{f}_o - \nabla P + \eta \nabla^2 \vec{v}, \quad (14)$$

which is valid even for multi-phase fluid flow where the mass density ρ and the viscosity η can change discontinuously. Here, \vec{g} is the acceleration due to gravity, \vec{f}_e is the electromagnetic force density, \vec{f}_o incorporates other body force densities such as that due to surface tension, P is the local pressure, and η is the fluid viscosity. For an idealized system composed of a solid rigid object free from the influence of gravity, the electromagnetic force density is the only source of momentum ($\vec{f}_m = \vec{f}_e$) and global momentum is conserved.

2.3. Electodynamic postulates

The electodynamic postulates are bound by two constraints. First, by ignoring the variations in energy of the kinetic sub-system, the energy of the electodynamic sub-system must be self-contained ($\phi_e = 0$) to maintain an overall system that is thermodynamically closed [34]. This assumption does not preclude absorption of the electromagnetic wave in a material, but simply implies that any energy absorbed within the material remains associated by name with the electodynamic sub-system. This distinction is arbitrary [40, 45, 52, 53] and immaterial to the ultimate goal of predicting material displacement and deformation. Second, mass-energy equivalence [59, 60, 67] relates the momentum density \vec{G}_e and energy flux density \vec{S}_e within a constant. If we interpret the electromagnetic field as a fluid with an equivalent mass density $\rho_{eq} = W_e/c^2$ moving with a group velocity $\vec{v}_g = \vec{S}_e/W_e$, the momentum density associated with the mass-equivalent field is given by $\vec{G}_e = \rho_{eq} \vec{v}_g$. This leads to an alternative statement of mass-energy equivalence

$$\vec{G}_e = \frac{\vec{S}_e}{c^2}. \quad (15)$$

Equation (15) has been historically acknowledged as Planck's theorem on the inertia of energy [68, 69]. When invoked, it achieves a symmetric energy-momentum tensor (or 4-vector) that is in compliance with angular momentum conservation [10, 34, 40, 70] and center-of-mass velocity conservation [37]. Equation (15) has since been widely used as a fundamental assumption in many field-based descriptions of light-matter interactions [11, 71–75].

Given the requirement of a closed electodynamic sub-system, the electodynamic postulates are sufficiently constrained so that they can be fully specified in terms of momentum density, power flux, and stress tensor. We will use five historically significant sets of postulates, listed in table 1, based on the Minkowski, Abraham, Einstein–Laub, Amperian, and Chu formulations of electrodynamics. The momentum density $\vec{D} \times \vec{B}$ is associated with the Minkowski formulation, $\epsilon_0 \vec{E} \times \vec{B}$ with the Amperian formulation, and $\vec{E} \times \vec{H}/c^2$ with the Abraham, Einstein–Laub, and Chu formulations. The last three can be further distinguished by slight variations in their respective stress tensors. Although the Abraham stress tensor in table 1 has been written in a symmetric form relative to

the dyadic products, which is common in the literature [26, 45], Abraham's original work [6] presents the stress tensor in an asymmetric form identical to that of the Minkowski stress tensor [5]. So long as the analysis is restricted to linear and isotropic materials, this difference is immaterial [76]. Symmetry of the energy-momentum tensor (equation (15)) is satisfied by only the Abraham, Einstein–Laub, Amperian, and Chu postulates. The Minkowski postulates form an energy-momentum tensor that is asymmetric, which has been argued to exclusively satisfy relativistic transformations [73, 77]. On the other hand, the Minkowski postulates can be made to form an energy-momentum tensor that is symmetric—a necessary condition to satisfy conservation of angular momentum and center-of-mass velocity—if we assume equation (15) supersedes the Poynting theorem and allow power flux to take on forms different from $\vec{E} \times \vec{H}$ [78]. To gain a fuller picture, our analysis will consider both symmetric and asymmetric forms of the Minkowski energy-momentum tensor, recognizing that there may be trade-offs in their consistency with other physical principles.

Although differences in momentum density amongst the postulate sets have received the most attention, it is just one facet of a complete electrodynamic theory. For example, the widely recognized Lorentz force density, $\vec{f} = \rho_e \vec{E} + \vec{J} \times \vec{B}$, can be derived in a non-magnetic medium through momentum continuity applied to the Amperian postulates for momentum density and stress tensor [64, 79]. The intuitive appeal of the Lorentz force density could be used as an indirect argument for the correctness of the Amperian postulates over other postulates, although the most definitive proof of any single set of postulates must rest on accord with experimental observations. The interconnectedness of the postulates listed in table 1 implies that debates over the momentum density in matter also impact the densities of energy, power, force, and stress, and we must be open to question even well-accepted postulates such as the Poynting vector or the Lorentz force density [62, 80] until conclusive empirical validation has been achieved.

3. Application of theory

Mutual interaction between fields and moving bodies (composed of either solids or liquids) is described in a simulation testbed that solves equations of electrodynamics and continuum dynamics with arbitrarily fine spatial and temporal resolution. Simulations help bridge a significant divide between electrodynamic theories and experimental measurements in several ways. First, it can be used to virtually replicate past radiation pressure experiments with a high degree of fidelity, leading to theoretical predictions of greater precision than those based on simplified models or approximate analytical expressions. Second, it offers a platform to compare testable predictions made by multiple electrodynamic postulates on equal footing. These comparisons are transparent because electrodynamic equations are numerically solved in their purest and most general form, as opposed to analytical solutions requiring intermediate steps and simplifying assumptions. Third, simulations allow dynamic visualization of

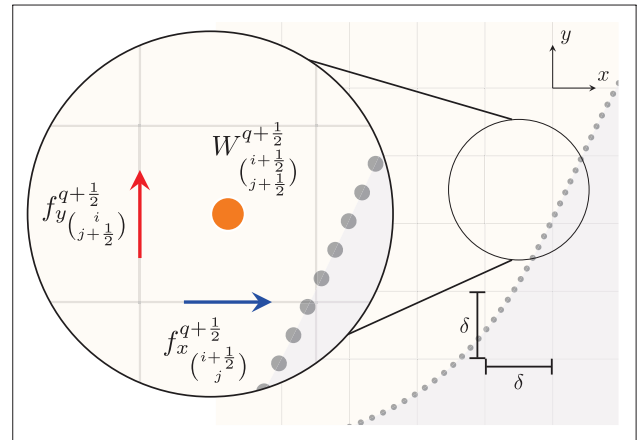


Figure 1. Placement of discretized electromagnetic force density and energy density over a two-dimensional Yee grid indexed in space by i and j and indexed in time by q . Positions of the discretized quantities are referenced by either whole or half increments of i , j , and q depending on where they fall on two staggered sub-grids that constitute the Yee grid. For multi-phase fluids, we use the front-tracking Marker and Cell method to define the boundary between fluids using marker points spaced by sub-cell distances.

electromagnetic and material quantities which are not directly accessible by experiments, providing greater context with which to interpret observable phenomena.

We combine standard numerical algorithms to solve the collection of equations that govern the electrodynamic and kinetic sub-systems. The electromagnetic fields are discretized on a fixed Yee grid with regular spacing δ in which fields of electric origin (\vec{E}, \vec{D}) and those of magnetic origin (\vec{H}, \vec{B}) are offset from each other by half-steps in space and time. Materials within the simulation domain are defined by specifying permittivity and permeability values on the electric and magnetic nodes, respectively. Using the finite-difference time-domain (FDTD) algorithm [81], the spatial and temporal derivatives in Maxwell's equations are approximated by second-order central-difference schemes, which enable updated electric and magnetic field values to be computed in lockstep based on past values. The boundaries of the simulations are described by a perfectly matched layer which completely absorbs incoming electromagnetic waves.

Because electromagnetic energy and momentum are generally defined by multiplication of electric and magnetic field quantities, it is necessary to perform simple averaging of the discretized fields \vec{E} , \vec{H} , \vec{D} , and \vec{B} so that they are defined at every half-step of the Yee grid. The momentum and energy continuity equations are approximated using central-difference schemes in both space and time, which feed off electrodynamic quantities strategically placed on the Yee grid. Considering a two-dimensional simulation domain for transverse-magnetic (TM) polarization, figure 1 illustrates a particularly efficient placement of the force and energy densities assuming two spatial dimensions in the xy plane indexed by (i,j) and one temporal dimension indexed by q . Discretization of the energy and momentum continuity equations according to this scheme yields the following update equations for the force and energy densities

$$f_x^{q+\frac{1}{2}} = -\frac{1}{\delta} \left[T_{xx}^{q+\frac{1}{2}} \left(\begin{array}{c} i \\ j+\frac{1}{2} \end{array} \right) - T_{xx}^{q+\frac{1}{2}} \left(\begin{array}{c} i+\frac{1}{2} \\ j+\frac{1}{2} \end{array} \right) + T_{xy}^{q+\frac{1}{2}} \left(\begin{array}{c} i \\ j+1 \end{array} \right) - T_{xy}^{q+\frac{1}{2}} \left(\begin{array}{c} i \\ j \end{array} \right) \right] \\ + \frac{1}{\Delta t} \left[G_x^{q+1} \left(\begin{array}{c} i \\ j+\frac{1}{2} \end{array} \right) - G_x^q \left(\begin{array}{c} i \\ j+\frac{1}{2} \end{array} \right) \right], \quad (16)$$

$$f_y^{q+\frac{1}{2}} = -\frac{1}{\delta} \left[T_{yx}^{q+\frac{1}{2}} \left(\begin{array}{c} i+1 \\ j \end{array} \right) - T_{yx}^{q+\frac{1}{2}} \left(\begin{array}{c} i \\ j \end{array} \right) + T_{yy}^{q+\frac{1}{2}} \left(\begin{array}{c} i+\frac{1}{2} \\ j+\frac{1}{2} \end{array} \right) - T_{yy}^{q+\frac{1}{2}} \left(\begin{array}{c} i-\frac{1}{2} \\ j+\frac{1}{2} \end{array} \right) \right] \\ + \frac{1}{\Delta t} \left[G_y^{q+1} \left(\begin{array}{c} i \\ j \end{array} \right) - G_y^q \left(\begin{array}{c} i \\ j \end{array} \right) \right], \quad (17)$$

and

$$W^{q+\frac{1}{2}} \left(\begin{array}{c} i+\frac{1}{2} \\ j+\frac{1}{2} \end{array} \right) = W^{q-\frac{1}{2}} \left(\begin{array}{c} i+\frac{1}{2} \\ j+\frac{1}{2} \end{array} \right) - \frac{\Delta t}{\delta} \left[S_x^q \left(\begin{array}{c} i+1 \\ j+\frac{1}{2} \end{array} \right) - S_x^q \left(\begin{array}{c} i \\ j+\frac{1}{2} \end{array} \right) + S_y^q \left(\begin{array}{c} i+\frac{1}{2} \\ j+1 \end{array} \right) - S_y^q \left(\begin{array}{c} i+\frac{1}{2} \\ j \end{array} \right) \right], \quad (18)$$

where Δt is the temporal step size. Such a prescription enables calculation of electromagnetic force and energy densities by programmatic insertion of different electrodynamic postulates, specified in terms of momentum density, stress tensor, and energy flux density (listed in table 1). This approach makes no simplifying approximations, save for discretization of space and time, and can directly solve the continuity equations for arbitrary configurations of materials and electromagnetic fields, which ensures compliance with conservation of energy and momentum. It should be noted that force densities calculated using momentum density and stress tensor offers an identical, but more transparent, means of comparing different postulates than explicit force density expressions [56, 82–86]. The forms of momentum density and stress tensor associated with each postulate set are both simple and incontrovertible, while questions have been raised about the physical significance of terms that appear in derived force density expressions [80, 84, 87].

We model the motion of objects under radiation pressure using either rigid body dynamics or fluid dynamics. The former applies to solid objects that experience negligible acceleration and deformation due to radiation pressure [49, 50, 55, 83, 88, 89], whereas the latter applies to fluid objects whose deformation under radiation pressure can subsequently alter the distribution of electromagnetic force density [54, 58, 90]. Multi-phase fluid dynamics are described by solving the incompressible Navier–Stokes equation on a coarser grid with regular spacing Δ using a front-tracking Marker and Cell (MAC) method [91, 92], which distributes velocity, density, and pressure on a staggered grid and defines the boundary between fluids as a contour with sub-cell resolution.

Interaction between electromagnetic fields and deformable fluids is described in a feedback loop cyclically modelling each on its relevant time scales under quasi-static conditions.

The time-averaged electromagnetic force density calculated using the FDTD method acts as a body force in the MAC method, which then determines the deformation of the fluid under the combined influence of gravity, radiation pressure, surface tension, and viscous forces. Once the front interface separating the two fluids has displaced one coarse grid spacing Δ , the fluid boundaries are updated on the Yee grid, and the time-averaged electromagnetic force density (averaged over at least 30 cycles) is re-computed. In this way, the FDTD and MAC solvers progress in turn, feeding each other updated distributions of the force density and interface at the end of their turns. The result is a series of detailed snapshots of the evolution of fluid bodies under dynamically varying radiation pressure and material distribution.

4. Results

We conduct a comprehensive study of some of the most important radiation pressure experiments over the past century by numerically replicating and analyzing their results. Virtual replication of a large body of literature consolidates and modernizes knowledge in the context of electrodynamic degeneracy and paves the way for empirical validation of observable predictions made by different electrodynamic postulates, a key step towards determining a single true theory of electrodynamics.

4.1. Electromagnetic momentum and center-of-mass velocity conservation

An influential thought experiment that tilted the Abraham–Minkowski debate in favor of the Abraham energy-momentum tensor was proposed by Balazs [37, 93] on the basis of center-of-mass velocity conservation. The thought experiment begins by considering two closed systems in vacuum each containing two entities: an initially stationary reflection-less planar slab of refractive index n and mass M and a light pulse of mass $m \ll M$. The trajectory of the pulse is normal to the interfaces of the slab. In the first closed system, the pulse flies over the slab, resulting in global momentum mc and a constant center-of-mass velocity $mc/(m + M)$. In the second closed system, the pulse intercepts the slab and slows down to c/n inside the slab. Assuming that the pulse mass is unchanged upon entering the slab, equivalence of the mass centroid and momentum of the two closed systems imposed dual constraints while the pulse is in the slab: the slab must move with a velocity $(mc - mc/n)/(m + M)$ to conserve center-of-mass velocity, and the pulse must have, to first order of m , a momentum mc/n to conserve global momentum. The latter is consistent with the Abraham electromagnetic momentum density. The thought experiment has been widely revisited and its conclusions have been generally supported [26, 29, 31, 37, 43, 47, 88, 94, 95].

The Balazs thought experiment is a starting point for understanding how the momentum of fields are constrained by fundamental conservation laws applicable to both fields and matter. But it gives an incomplete picture. The thought experiment speculates on values of slab velocity and pulse

momentum only after the pulse has entered the slab but does not provide causal descriptions of how slab velocity and pulse momentum evolve toward these values. Such descriptions would require, at the very least, dynamic information about the force density applied to the slab. Moreover, the thought experiment imposes idealizations of the slab properties—the slab must neither reflect, absorb, nor refract—such that experimental validation is likely impossible. For a complete account of momentum transfer between fields and matter generalizable to experimentally feasible configurations, the conservation constraints imposed by the Balazs thought experiment must be paired with a field-based description of momentum and energy, which are governed by Maxwell's equations and any one of the sets of electrodynamic postulates. Such efforts were recently undertaken to analyze pulse interaction with a slab using the Einstein–Laub postulates, which were shown to provide a picture consistent with the conservation laws imposed by the Balazs thought experiment for cases in which the slab is reflective, lossy, dispersive, magnetic, or negative-index [55, 88, 96]. Here, we extend on these efforts to show that all five electrodynamic postulates can be made mathematically consistent with the conservation constraints of the Balazs thought experiment. This provides a generalization of the conclusions of recent work [97] showing the compatibility of the Abraham and Minkowski momentum densities with the thought experiment. We show that a subtle flaw in the logic of the original thought experiment biases its outcome towards the Abraham momentum density. Nonetheless, the postulates that pair with the Abraham momentum density (Abraham, Einstein–Laub, and Chu) can still be argued to be the most physical on the grounds of energy conservation across interfaces.

Mimicking the configuration considered in the original Balazs thought experiment, we simulate the dynamics of an initially stationary closed system consisting of a pulse, a massive, rigid slab, and an enclosure. We first consider the three sets of postulates (Abraham, Einstein–Laub, and Chu) that endorse the Abraham momentum density, fully expecting all conservation laws to be upheld. A short pulse is directed towards an impedance-matched positive-index slab from free space. The spatial length of the pulse has been chosen to be less than the thickness of the slab so that the pulse can be fully immersed in the slab and its interactions with the front and back of the slab can be distinguished in time. Figure 2 provides snapshots of the momentum and center-of-mass velocity contributions of the pulse, slab, and enclosure as the pulse is borne on the left side of the enclosure and absorbed on the right. As expected, the pulse imparts no net effect on the initially stationary closed system—the total momentum and center-of-mass velocity remain fixed at zero for all time. When the pulse is fully immersed in the slab, the dynamics of the pulse and slab match the predictions of the thought experiment. Slow-down of the pulse is compensated by a speed-up of the slab, while a decrease in pulse momentum is compensated by an increase in slab momentum. As expected, the three postulates based on the Abraham momentum density are consistent with fundamental conservation laws.

If we revisit the previous example using an asymmetric tensor made of the Minkowski momentum density and the

canonical Poynting vector (as presented in table 1), the pulse, slab, and enclosure dynamics conserve global momentum but not center-of-mass velocity. As shown in figure 2, the backward recoil of the slab upon pulse entry and the forward recoil upon pulse exit produces a net displacement of the entire system, an impossibility for a closed system of fixed stationary state. Violation of center-of-mass velocity conservation in this way has been widely used to discredit the Minkowski momentum density. However, it more correctly serves to implicate the asymmetric energy-momentum tensor formed by the combination of the Minkowski momentum density with the canonical Poynting vector. By pairing the Minkowski momentum density with its complimentary power flux $c^2\vec{D} \times \vec{B}$, the Minkowski postulates form a symmetric energy-momentum tensor that makes predictions fully compliant with global momentum and center-of-mass velocity conservation in polarizable and magnetizable media, as shown in figure 2. Similar arguments hold true for the Amperian momentum density, albeit restricted to magnetizable media. When paired with the canonical Poynting vector, the Amperian postulates do not generally conserve center-of-mass velocity. Pairing the Amperian momentum density with the power flux $\vec{E} \times \vec{B}/\mu_0$ resolves this problem, as shown in figure 2. Thus, the Minkowski and Amperian postulates—so long as they form symmetric energy-momentum tensors by pairing with power flux definitions in accordance equation (15)—can describe the evolution of momentum and energy in a way that satisfies the same conservation laws as those satisfied by the Abraham, Einstein–Laub, and Chu postulates.

Changing the definition of power flux enables momentum densities other than Abraham's to be consistent with center-of-mass velocity conservation, but it has consequences on the predicted distribution of electromagnetic energy, particularly at interfaces. The integral formulation of energy continuity applied to an infinitesimally thin pillbox straddling an interface mandates that any discontinuity of the normal component of power flux must drive a change in surface energy density. For transverse electromagnetic waves, discontinuous power flow across interfaces can occur if power flux is defined using either \vec{D} or \vec{B} , resulting in the deposition or extraction of energy at surfaces. This effect is illustrated by simulations in figure 3, which depicts three different forms of energy density (resulting from three different forms of power flux) applied to describe a pulse incident onto an impedance-matched (polarizable and magnetizable) slab. When the pulse is described by an energy density associated with the canonical Poynting vector $\vec{E} \times \vec{H}$, it glides through the slab without leaving a trace, a plausible picture of how a pulse should interact with a lossless, impedance-matched slab. On the other hand, when the pulse is described by energy densities associated with either $c^2\vec{D} \times \vec{B}$ or $\vec{E} \times \vec{B}/\mu_0$, stationary deficits and surpluses of energy at the slab entrance and exit, respectively, remain even after the passage of the pulse.

Surface energy densities at slab discontinuities are necessary for the Minkowski and Amperian postulates to achieve theoretical compliance with center-of-mass velocity conservation. For example, in the case of a pulse crossing the threshold

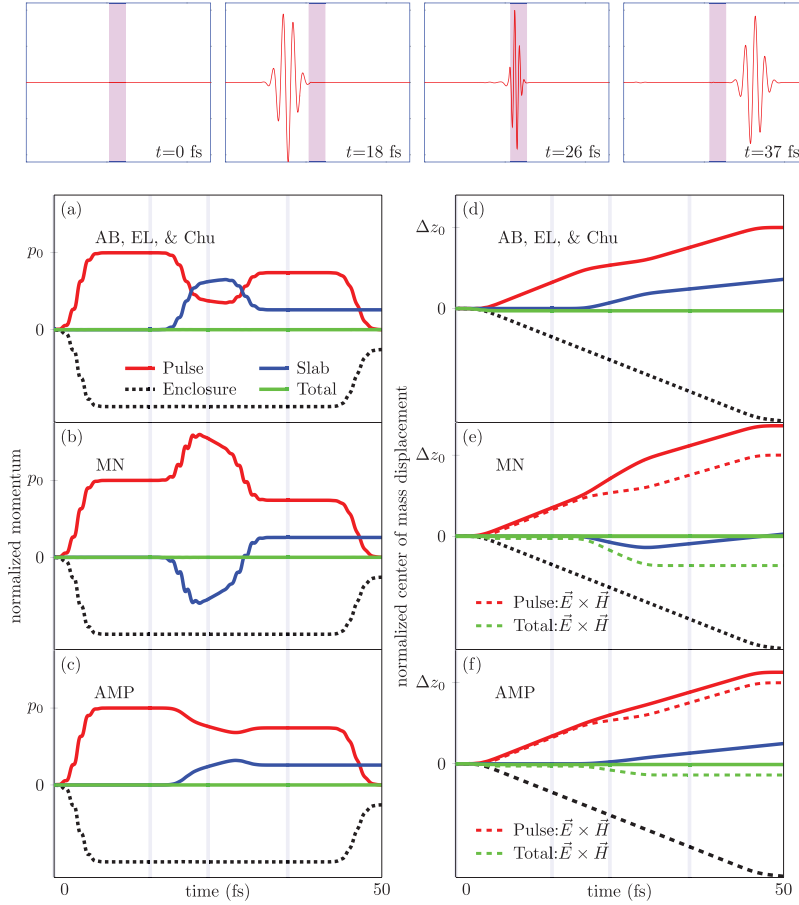


Figure 2. Consistency of the Minkowski (MN), Abraham (AB), Einstein–Laub (EL), Amperian (AMP), and Chu postulates with fundamental conservation laws visualized by pulse transmission through a slab. We consider a closed system consisting of an electromagnetic pulse, centered at a free-space wavelength $\lambda_0 = 632$ nm and pulse width $\tau = 2$ fs, incident onto an impedance-matched, dispersive slab of thickness $d = 1050$ nm, relative permittivity $\epsilon_r = 2.2$, and relative permeability $\mu_r = 2.2$. The pulse and slab are immersed in vacuum and contained in a rigid enclosure. (top row) Snapshots of the pulse electric field emitting from the left side of the enclosure, propagating through the slab, and disappearing on the right side of the enclosure. (left column) Momentum contained in the pulse (red), slab (blue), and enclosure (black) over the lifespan of the pulse as described by (a) the Abraham, Einstein–Laub, and Chu postulates, (b) the Minkowski postulates, and (c) the Amperian postulates. Momentum is referenced to the free-space momentum of the pulse, p_0 . The total momentum (green) is always fixed at zero as required by global momentum conservation. (right column) Center-of-mass displacement of the pulse (red), slab (blue), and enclosure (black) as described by (d) the Abraham, Einstein–Laub, and Chu postulates, (e) the Minkowski postulates using either $\vec{E} \times \vec{H}$ (dashed) or $\vec{D} \times \vec{B}$ (solid) as the power flux, and (f) the Amperian postulates using either $\vec{E} \times \vec{H}$ (dashed) or $\epsilon_0 \vec{E} \times \vec{B}$ (solid) as the power flux. The center-of-mass displacement is normalized to the net slab displacement divided by its mass ratio. The system center-of-mass (solid green) is always fixed at zero as required by center-of-mass velocity conservation. The system center-of-mass predicted by the Minkowski and Amperian postulates with the Poynting vector $\vec{E} \times \vec{H}$ (dashed green) strays from zero and thus, is inconsistent with center-of-mass velocity conservation.

between free space and a rigid polarizable and magnetizable slab, a backward slab recoil associated with an increase in Minkowski momentum is precisely and dynamically balanced out by a forward pulse recoil associated with an increase in pulse mass (or energy) the moment the pulse enters the slab. In a closed system with only fields and material, the only possible source of this increase is mass (or energy) extracted from the slab entrance. Without such mechanisms, general consistency with center-of-mass conservation using the Minkowski and Amperian postulates is not possible.

Since the surface energy densities predicted by the Minkowski and Amperian postulates have yet to be observed and are unlikely to exist in practice, the empirical validity of both postulate sets can rightly be challenged. Amperian power

flow descriptions, however, have been theoretically rationalized on the basis that fields in magnetizable media carry a portion of energy (and momentum) that is ‘hidden’ [10, 61, 98]—that is, purely mathematical and not observable in the physical world. The basis of such hidden energy is that the Amperian model of magnetization is fundamentally derived from current loops (as opposed to magnetic charge), which carry inherent self-sustaining energy. Empirical plausibility of the Minkowski postulates would require a similar notion of hidden energy, albeit extended to polarizable media. Such arguments have yet to be put forward. The postulates that require hidden energy concepts should be viewed with some skepticism, since hidden energy is not experimentally testable and alternative electrodynamic postulates exist that require no such considerations.

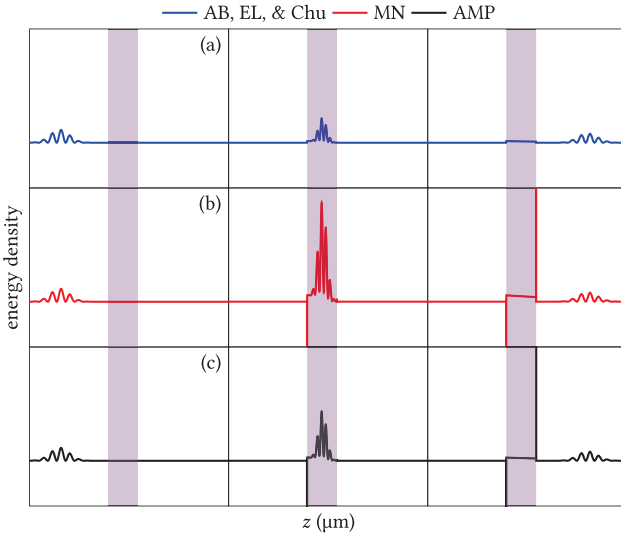


Figure 3. Instantaneous energy density distributions at three moments in time predicted by (a) the Abraham (AB), Einstein–Laub (EL), and Chu postulates, (b) the Minkowski (MN) postulates, and (c) the Amperian (AMP) postulates, for the case of a pulse normally incident onto a slab under conditions identical to those in figure 2.

We next model electrodynamic interaction between a pulse and slab in a closed two-dimensional system. Extension of the analysis to more than one dimension is important, as it incorporates additional sources of electromagnetic momentum associated with electrostriction, magnetostriction, field gradients, and out-of-plane scattering (refraction) that are unavoidable in any experimental implementation. To this end, we use all five sets of electrodynamic postulates to study two configurations in which a finite-width pulse strikes a tilted planar slab at 45° immersed in vacuum: one in which the slab is made of positive-index glass and the other in which it is made of a hypothetical negative-index medium. As shown in figure 4, global momentum and center-of-mass velocity are conserved using all five postulates regardless of whether the pulse undergoes positive or negative refraction in the slab, re-affirming the conclusions reached by studying one-dimensional pulse-slab interactions. This example also shows that force density calculations using momentum density and stress tensor are complete and consistent with global momentum and center-of-mass velocity conservation even in complex multi-dimensional configurations. Separation of force density terms to explicitly describe the effects of scattering and field gradients [89] may provide intuitive appeal, but is ultimately unnecessary and, unless explicitly checked, threatens total harmony with conservation laws.

As shown in figures 4 and 5, the five postulates make different predictions of the slab recoil and therefore, can potentially be distinguished by experiments. For the case of a glass slab, for example, the Minkowski postulates predict a momentary backward slab recoil, whereas all other postulates predict a forward slab recoil. This difference could be observed using short pulses in which recoil imbalances upon pulse entry and exit are separated in time, a proposal bearing some similarity to a recent suggestion to differentiate the Abraham and Minkowski forces based on the torque imparted

by a series of short pulses sent through a cylindrically wound wire [99]. Measurements of pulse-induced recoil have yet to be performed, but, according to these simulations and some of the recent literature, hold promise for empirical validation of a unique electrodynamic theory.

4.2. Radiation pressure on submerged mirrors

Successive experiments in the early 1900s, first by Lebedev [2], then by Nichols and Hull [3, 4], and later by Bell and Green [100], provided evidence that light impinging from vacuum could transfer momentum to macroscopic objects. It was not until the mid-1900s that attempts were made to probe the momentum conferred by light impinging from dielectric media. In 1954, Jones and Richards [12] immersed a rhodium-coated silver mirror in various dispersive liquids ranging in refractive index from 1.33 to 1.63 and observed its displacement caused by illumination using a tungsten lamp. They concluded that light of a fixed intensity exerted a normalized pressure that is proportional to the refractive index of the liquids within an error of $\pm 1.2\%$. This experiment was later refined in 1978 by Jones and Leslie [13]. The lamp was replaced with a HeNe laser to increase light coherence, and the rhodium-coated silver mirror was replaced with a multi-layered dielectric mirror (of unknown composition) to mitigate heating and thermal expansion. Improved experimental precision yielded confirmation, within a reduced error of $\pm 0.05\%$, of a linear dependence of normalized radiation pressure on the refractive index of the immersing fluids.

Although the results of the Jones–Richards and Jones–Leslie experiments are most directly explained by light momentum of the Minkowski form [24–27], there has been growing evidence that the experiments could be modelled using different electrodynamic formulations [46, 48, 101–104]. As early as 1978, Jones [46] proposed a model to explain momentum transfer to submerged mirrors as originating from an Abraham-like momentum tied to the fields and a remaining portion tied to mechanical perturbations in the dielectric, both of which sum up to give a Minkowski-like total momentum. Field-based descriptions of the experiments have accurately predicted the dependence of radiation pressure on refractive index using the Einstein–Laub postulates [103], the Minkowski and Chu postulates [27, 104], and the Lorentz force density [101, 102]. These efforts, in turn, have been used as evidence in support of the Abraham momentum density [103], the Minkowski momentum density [27, 104], or the arithmetic mean of the two [101, 102]. Consolidation of these diverse interpretations remains a challenge.

Depending on the starting electrodynamic postulates, different routes can be taken to arrive at identical predictions of radiation pressure. This is illustrated by considering pulse interaction with a reflective mirror assumed to be a perfect electric conductor, a common approximation of the mirrors used in the Jones–Richards and Jones–Leslie experiments [27, 48, 103]. The pulse, mirror, and surrounding dielectric medium are encased in an enclosure that is closed and initially stationary such that (1) dynamic redistribution of

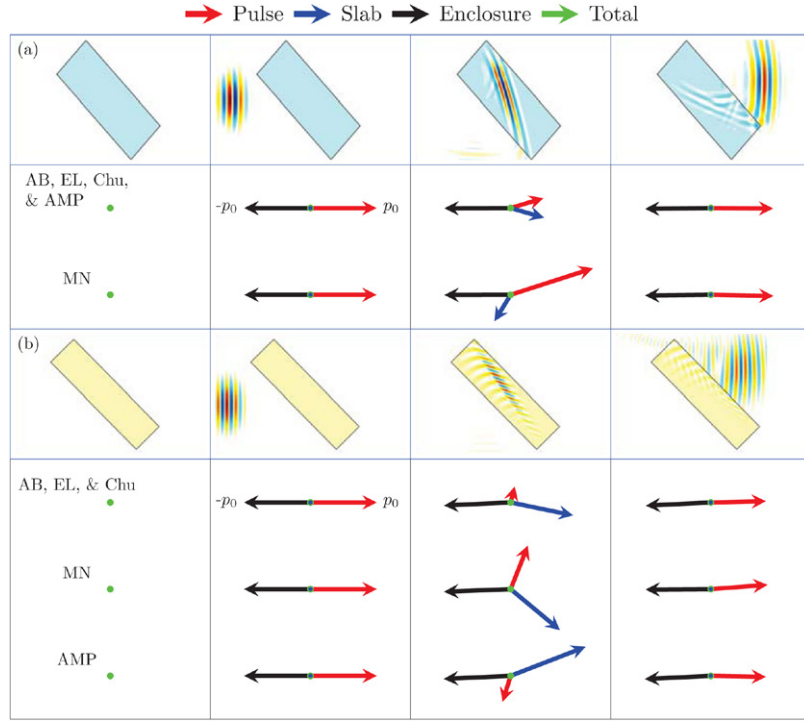


Figure 4. Two-dimensional field-based implementation of the Balazs thought experiment. Non-degenerate momentum predictions made by the Minkowski (MN), Abraham (AB), Einstein–Laub (EL), Chu, and Amperian (AMP) postulates for closed systems in which finite pulses are obliquely incident onto tilted impedance-matched slabs having (a) $n = \sqrt{3}$ (blue) and (b) $n = -1.3 + i0.07$ (yellow). The vector diagrams show instantaneous momentum of the pulse (red arrow), slab (blue arrow), enclosure (black arrow), and total system (green arrow) as the pulse propagates through the slabs. The total system momentum is conserved for all cases, as indicated by the stationary green dots. Slab thicknesses ($d = 5250$ nm for the positive-index slab and $d = 3500$ nm for the negative-index slab) have been chosen so that the incident pulse ($\lambda_0 = 500$ nm, $\tau = 2$ fs) is fully immersed in the slab prior to exit. Dispersion of the negative-index slab is described by a Drude model for the permittivity and permeability with the following parameters: scattering rate $\Gamma = 2250$ THz, plasma frequency $\omega_p = 1200$ THz, static permittivity $\varepsilon_\infty = 1.4$, and static permeability $\mu_\infty = 1.4$.

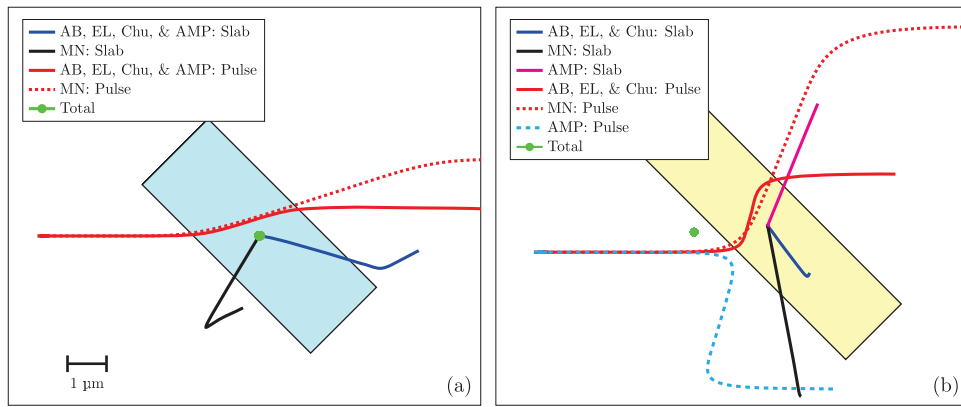


Figure 5. Non-degenerate center-of-mass displacement predictions made by the Minkowski (MN), Abraham (AB), Einstein–Laub (EL), Chu, and Amperian (AMP) postulates for closed systems in which finite pulses are obliquely incident onto tilted impedance-matched slabs having (a) $n = \sqrt{3}$ (blue) and (b) $n = -1.3 + i0.07$ (yellow). The configurations are identical to those in figure 4. Note that total center-of-mass displacement remains fixed, as indicated by the stationary green dots.

momentum must always achieve a zero sum and (2) the origins of the mirror momentum can be visualized in time. We assume that the surrounding medium and enclosure are connected. A finite-duration pulse of longitudinal spatial extent less than the extent of the immersing dielectric is unleashed from the left end of the enclosure and bounces off the mirror at normal incidence. As shown in figure 6, the postulates predict dynamics that are all consistent with global

momentum conservation and indistinguishable except for one. The Minkowski postulates, the lone outlier, describe the transfer of momentum upon reflection as a two-body process involving just the pulse and mirror. The pulse is created with momentum np_0 and the system recoils with equal and opposite momentum $-np_0$, where p_0 is the momentum of the pulse in vacuum. With the system momentum fixed at $-np_0$ over the remaining duration of the simulation, the pulse confers

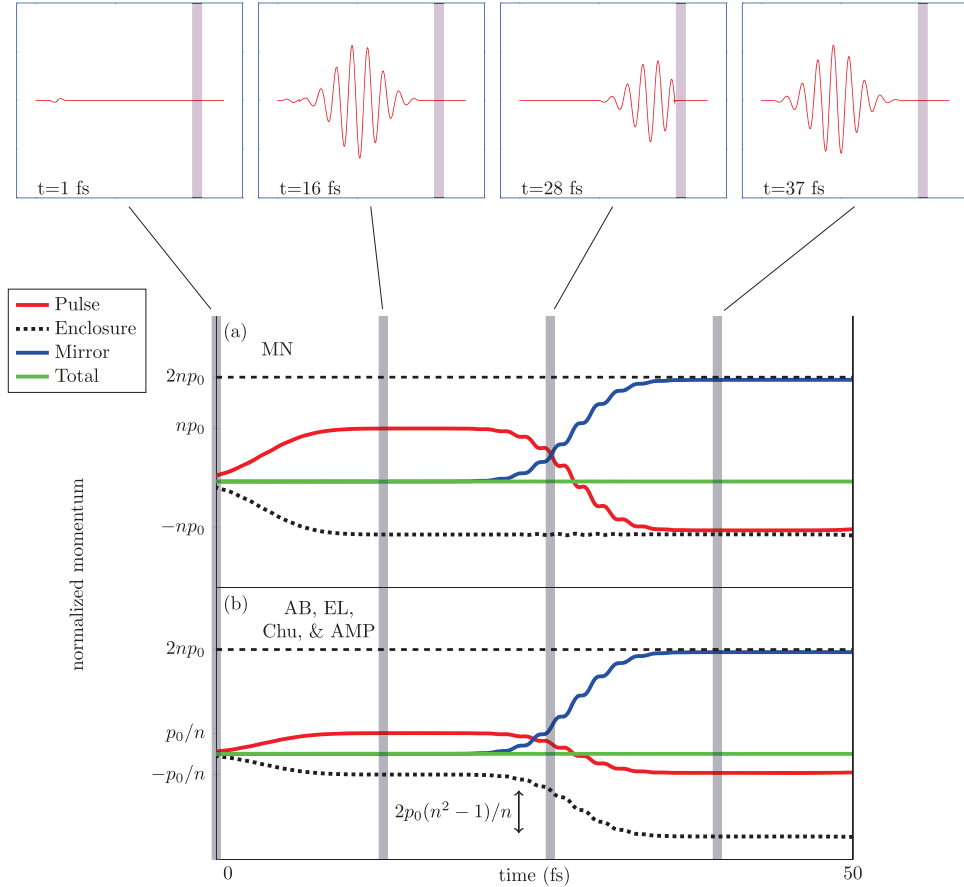


Figure 6. Instantaneous momentum transfer between a pulse ($\lambda_0 = 632 \text{ nm}$, $\tau = 2 \text{ fs}$), an enclosure containing a fluid ($n = 1.6$), and a submerged mirror approximated as a perfect electric conductor. The top panel shows simulation snap-shots of the electric field as the pulse reflects from the mirror. The momentum of the pulse (red solid line), enclosure and the surrounding fluid (black dotted line), mirror (blue solid line), and total system (green solid line) predicted by (a) the Minkowski postulates and (b) the Abraham, Einstein–Laub, Chu, and Amperian postulates. All five postulates predict the same final slab momentum of $2np_0$. Note that the enclosure and surrounding fluid are connected such that momenta associated with both are lumped together.

momentum $2np_0$ directly to the mirror upon reflection. The other postulates (Abraham, Einstein–Laub, Amperian, Chu) describe the transfer of momentum as a three-body process involving the pulse, surrounding fluid, and the mirror. The pulse is created with momentum p_0/n and the system recoils with momentum $-p_0/n$. When the pulse reflects from the mirror, two mechanisms transfer momentum to the mirror. The mirror receives a parcel of momentum $2p_0/n$ due to reversal of the pulse direction and another parcel of momentum $2(n^2 - 1)p_0/n$ present in the surrounding fluid, resulting in a final mirror momentum $2np_0$. Because the final mirror momentum for all postulates is the same, and differences in the mediating mechanisms are likely immeasurable, the five postulates in this case are degenerate.

Lorentz force calculations of radiation pressure on a submerged reflector imparting arbitrary phase have shown that the acquired momentum can vary continuously with phase between an upper bound of the Minkowski momentum and a lower bound of the Abraham momentum [101, 102]. Pulse interaction with a perfect magnetic conductor—the compliment of a perfect electric conductor—illustrates how a half-cycle phase shift in the reflected electric field can drastically alter radiation

pressure predictions. As shown in figure 7, repeating the previous example using a perfect magnetic conductor shows that all postulates remain faithful to global momentum conservation, but degeneracy of the final mirror momentum has now been broken. The Minkowski and Abraham postulates predict a final mirror momentum $2np_0$ resulting from either two-body or three-body momentum transfer processes upon pulse reflection. The Einstein–Laub, Chu, and Amperian postulates, on the other hand, predict a smaller final slab momentum of $2p_0/n$, which is acquired directly by the reversal of the pulse momentum without the accompanying system recoil observed for the case of a perfect electric conductor.

Given that radiation pressure on submerged mirrors is not completely degenerate and can be phase dependent, accurate modelling of the Jones–Richards and Jones–Leslie experiments must fully account for the specific configurations in which radiation pressure is generated. We use the five electrodynamic postulates in simulations that describe the two experiments to a degree of realism unmatched to date. The simulations incorporate realistic experimental conditions such as broadband illumination, the skin effect in a metallic mirror, multiple reflections in a dielectric mirror, and frequency-dependent

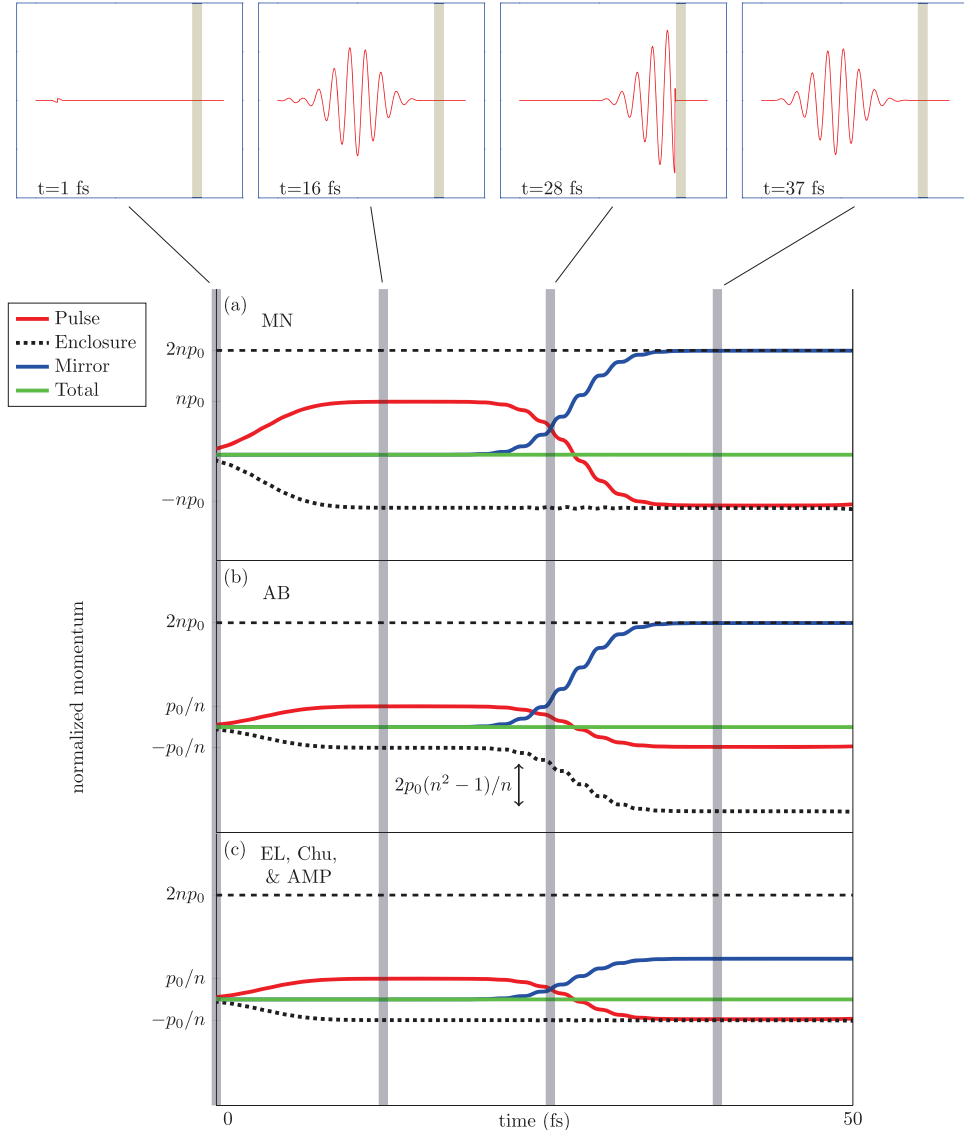


Figure 7. Instantaneous momentum transfer between a pulse ($\lambda_0 = 632$ nm, $\tau = 2$ fs), an enclosure containing a fluid ($n = 1.6$), and a submerged mirror approximated as a perfect magnetic conductor. The top panel shows simulation snap-shots of the electric field as the pulse reflects from the mirror. The momentum of the pulse (red solid line), enclosure and the surrounding fluid (black dotted line), mirror (blue solid line), and total system (green solid line) predicted by (a) the Minkowski postulates, (b) the Abraham postulates, and (c) the Einstein–Laub, Chu, and Amperian postulates. The Minkowski and Abraham postulates predict a final slab momentum of $2np_0$, whereas the Einstein–Laub, Chu, and Amperian postulates predict a final slab momentum of $2p_0/n$. Note that the enclosure and surrounding fluid are connected such that momenta associated with both are lumped together.

dispersion. To mimic power normalization used in both experiments, the incident time-averaged power flux for each case of immersing fluid is kept constant, a consideration whose importance has been recently pointed out [103].

We begin by considering the Jones–Richards experiment in which incoherent, broadband light from a tungsten lamp illuminates a rhodium-coated silver mirror. Virtual replication of the original experiment is limited by missing information, such as the spectral distribution of the tungsten lamp, the complex permittivity of the rhodium-coated silver, and the thicknesses of rhodium and silver. In the absence of these details, we make the reasonable assumption that the mirror is made from either bulk rhodium or bulk silver, modelling each metal by fitting the Drude model to experimentally measured

permittivity values found in [105] for rhodium and [106] for silver. The tungsten light source is modelled as a summation of incoherent plane waves with a Gaussian spectral distribution centered at the wavelength 632 nm. Key assumptions of the analysis, including the Drude model fits to permittivity values of rhodium and silver and the assumed spectral distribution of the tungsten light source, are shown in figure 8.

Radiation pressure on a submerged metallic mirror predicted by different postulates can change dramatically depending on the assumed properties of the mirror. As shown in figure 9(a), if the mirror is assumed to be a perfect electric conductor, all five postulates identically predict pressure that linearly scales with the fluid index, a result that matches the experimental data within error. Not surprisingly, the predicted pressure becomes

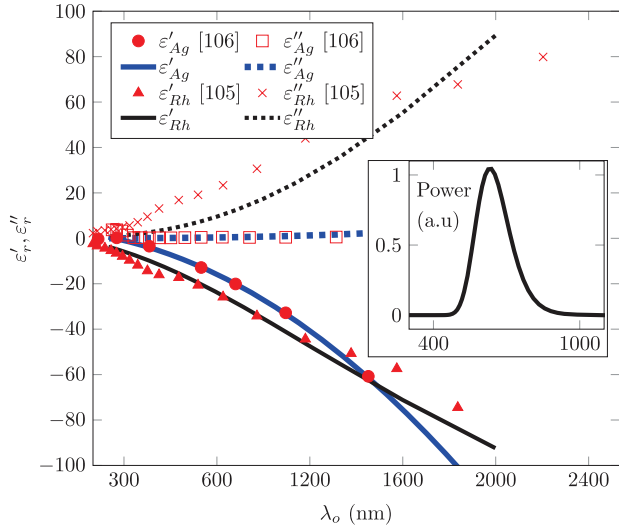


Figure 8. Key assumptions used to model the Jones–Richards experiment. The real part of complex permittivity ε' (solid lines) and the imaginary part of the complex permittivity ε'' (dotted lines) produced by the Drude model when fitted to tabulated permittivity values of rhodium (markers: triangle, cross) [105] or silver (markers: circle, square) [106]. The inset depicts the power spectrum of a broadband incoherent light source assumed to emulate light from the tungsten lamp used in the Jones–Richards experiment.

inversely proportional to fluid index for the Einstein–Laub, Chu, and Amperian postulates when the perfect electric mirror is replaced by a perfect magnetic mirror. However, when we model the metallic mirror as a dispersive metal, the coincidence between theory and experiment seen before by assuming a perfect electric conductor is weakened. Incorporating the dispersion of the metal introduces two realistic effects: losses in the metal and a slight, but non-zero, phase shift imparted by reflection. As shown in figure 9(b), the pressures predicted by all five postulates exhibit departures from the Jones–Richards experimental data that become significant for higher fluid index values. This departure is even more pronounced if the mirror is rhodium as opposed to silver, due to the larger optical losses of rhodium which fall further from the perfect electric conductor approximation. For identical simulation parameters, the Einstein–Laub, Chu, and Amperian postulates are generally in worse agreement to the experimental data than the Abraham and Minkowski postulates. However, without detailed knowledge of the exact composition of the rhodium-coated silver mirror, it is not possible to conclude whether any of the postulates accurately predict the Jones–Richards results. Further radiation pressure measurements using well-characterized metallic mirrors are thus a necessary step towards the isolation of an electrodynamic theory.

We next consider the Jones–Leslie experiment in which coherent radiation from a laser illuminates a submerged dielectric layered mirror, resulting in pressure scaling linearly with fluid index. Again, virtual replication of the original experiment is limited because the composition of the dielectric mirror (which was purchased from a vendor) was not reported. Here, we assume a dielectric mirror made from alternating, quarter-wavelength-thick layers of MgF_2 ($n = 1.37$) and

ZnS ($n = 2.35$), a recipe reported by Jones and Leslie [13] to make some of the other mirrors used in their experiment. Interestingly, the ordering of the layers can significantly alter the radiation pressure predicted by some of the postulates, as shown in figure 9(c). The Abraham and Minkowski postulates predict n -proportional radiation pressure regardless of the layer ordering, but the other three postulates predict either n -proportional or $1/n$ -proportional radiation pressure depending on whether the higher-index layer (ZnS) or the lower-index layer (MgF_2) is the exterior layer in contact with the surrounding fluid. The sensitivity of the radiation pressure to the layer ordering arises from the phase variations in the reflection from a dielectric mirror. That is, the phase of reflection from a dielectric mirror when capped by the higher-index layer is like that from a perfect electric mirror. When capped by the lower-index layer, it is like that from a perfect magnetic mirror. Without knowing the composition of the dielectric mirror used in the Jones–Leslie experiment, we cannot rule out any of the postulates on the basis of the experimental accord, since all postulates are capable of predicting n -proportional radiation pressure in agreement with the experimental data. In light of this analysis, an essential experiment to test the hypothesis of phase-dependent radiation pressure is to measure the radiation pressure difference on two submerged dielectric mirrors whose layers are ordered differently but otherwise identical.

An important conclusion of the Jones–Leslie experiment is that radiation pressure is dependent on the phase refractive index as opposed to the group refractive index. We simulate the pressure on dielectric mirrors (with a low-index capping layer) immersed in fluids that are modelled as dispersive dielectrics with variations in group and phase refractive indices matching those reported by Jones and Leslie [13]. As shown in figure 9(d), adding the effect of dispersion to the surrounding fluid medium has a negligible effect on the pressure trends for all postulates, which remain dependent on phase refractive index.

Interpretations of radiation pressure on submerged mirrors are muddled by the presence of force densities residing in the adjacent fluid. There is no consensus on the importance of these contributions to the total radiation pressure on the mirror, as they have been neglected by some [103] and incorporated by others [104, 107]. To illustrate their relative importance for each of the five postulates, figures 10(a) and (b) plot the time-averaged force density exerted by a normally incident continuous wave onto a multi-layered dielectric mirror capped by a low-index layer and a high-index layer, respectively. The Minkowski and Abraham postulates predict a series of pressure spikes localized at the interfaces of the dielectric mirror but no force density in the fluid region. The Einstein–Laub, Chu, and Amperian postulates, on the other hand, predict oscillatory force density patterns that span across the fluid and dielectric mirror regions. Consistent with previous observations, the force density in the dielectric mirror is larger when the mirror is capped by the higher-index layer. The force density in the fluid region can add or subtract to the total radiation pressure on the submerged mirror. As shown in figure 11, the pressure on the mirror oscillates between n and $1/n$ by accounting for force density residing in every quarter cycle

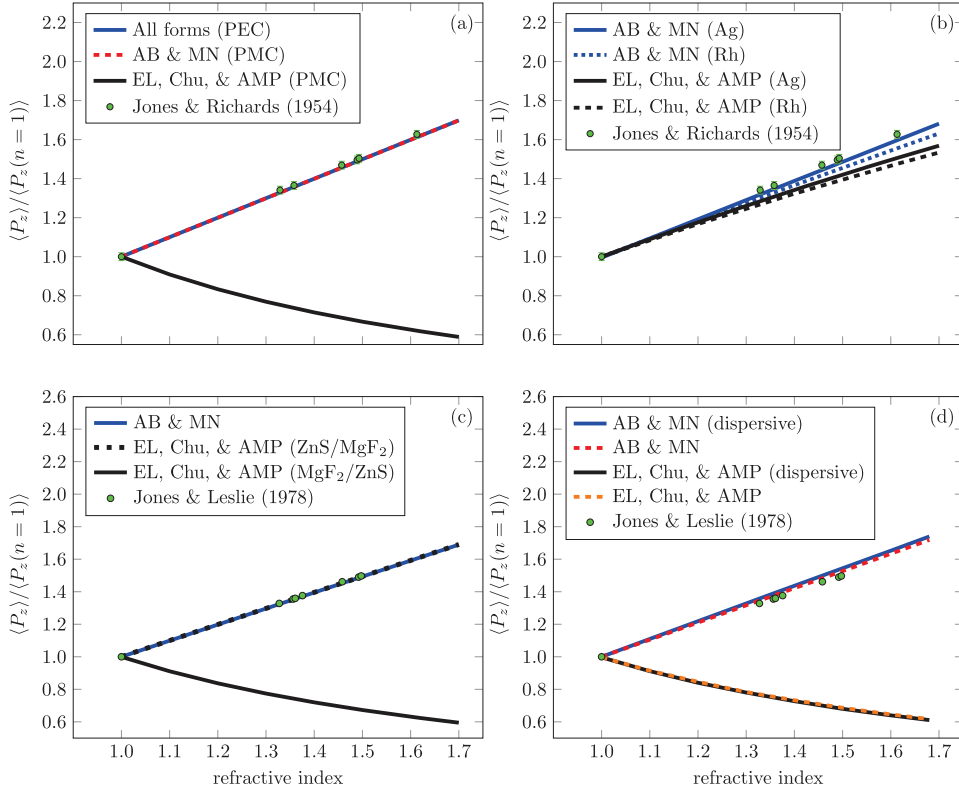


Figure 9. Normalized time-averaged radiation pressure on submerged mirrors predicted by the Minkowski (MN), Abraham (AB), Einstein–Laub (EL), Chu, and Amperian (AMP) postulates. The green dots and error bars in (a) and (b) are data from the 1954 Jones–Richards experiment. The green dots in (c) and (d) are data from the 1978 Jones–Leslie experiment. Note that the error in the 1978 Jones–Leslie experiment is smaller than the dot size. The mirrors, immersed in fluids with refractive index n that varies from 1.0 to 1.7 in steps of 0.1, are illuminated at normal incidence. Pressure predictions are made for the following cases: (a) A perfect mirror (electric or magnetic) submerged in fluids without dispersion; (b) a mirror made of dispersive silver or rhodium (whose permittivity is modelled using the Drude model fitted to tabulated data [105, 106]); (c) a multi-layered dielectric mirror composed of alternating quarter-wavelength-thick layers of MgF₂ (refractive index 1.38) and ZnS (refractive index 2.35) submerged in fluids without dispersion for configurations in which the outermost dielectric layer is MgF₂ (MgF₂/ZnS) or ZnS (ZnS/MgF₂); (d) a multi-layered (MgF₂/ZnS) dielectric mirror where the amount of dispersion in the fluids is set to $n_g \approx 1.03n$, where n_g is the group refractive index and n is the phase refractive index (corresponding to the maximum upper bound of the fluid dispersion as reported by Jones and Leslie [13]). The mirrors in (a) and (b) are illuminated at normal incidence by an incoherent white light source with spectral intensity shown in the inset of figure 8, which approximates the spectral distribution of light from a tungsten lamp. The mirrors in (c) and (d) are illuminated at normal incidence by monochromatic radiation at the wavelength $\lambda_0 = 632.8$ nm.

into the fluid, matching similar predictions made in [48, 101]. Depending on the ordering of the layers, the radiation pressure either decreases from n to $1/n$ or increases from $1/n$ to n by adding force density contributions within the first quarter cycle into the fluid. This adds an additional layer of complexity to the interpretation of the Jones–Leslie experiments, as the observed index proportionality of radiation pressure measured by Jones and Leslie can be recovered by the Einstein–Laub, Chu, and Amperian postulates through selective force density integration into the fluid.

4.3. Laser-driven liquid interface deformation

Perhaps the simplest configuration to probe the momentum of light is to observe its passage across the threshold between vacuum and a dielectric medium. Changes in the momentum of light upon entering the medium should be offset by an on-axis recoil dependent on whether momentum takes on Minkowski or Abraham forms [36, 58]. For the simple case of a beam of intensity I normally incident from air onto a

dielectric medium of refractive index n , the Minkowski form of momentum predicts a negative pressure (pull) of [36]

$$P = -\frac{2I}{c} \frac{n-1}{n+1}, \quad (19)$$

whereas the Abraham form of momentum predicts a positive pressure (push) of

$$P = \frac{2I}{c} \frac{n-1}{n+1}. \quad (20)$$

In 1973, Ashkin and Dziedzic [14] implemented an experiment to measure the longitudinal recoil exerted by pulses entering a deformable dielectric medium. In their experiment, an air–water interface was illuminated with high-power (3 kW), 60 ns-long, 530 nm-wavelength laser pulses focused down to a spot size of radius 2 μm . Based on the far-field profile of the transmitted pulse, it was inferred that the pulse induced a momentary, micron-scale, upward bulge on the water surface, overcoming both surface tension ($\approx 7 \text{ mJ m}^{-2}$ at room temperature) and gravity. The direction of the bulge, consistent

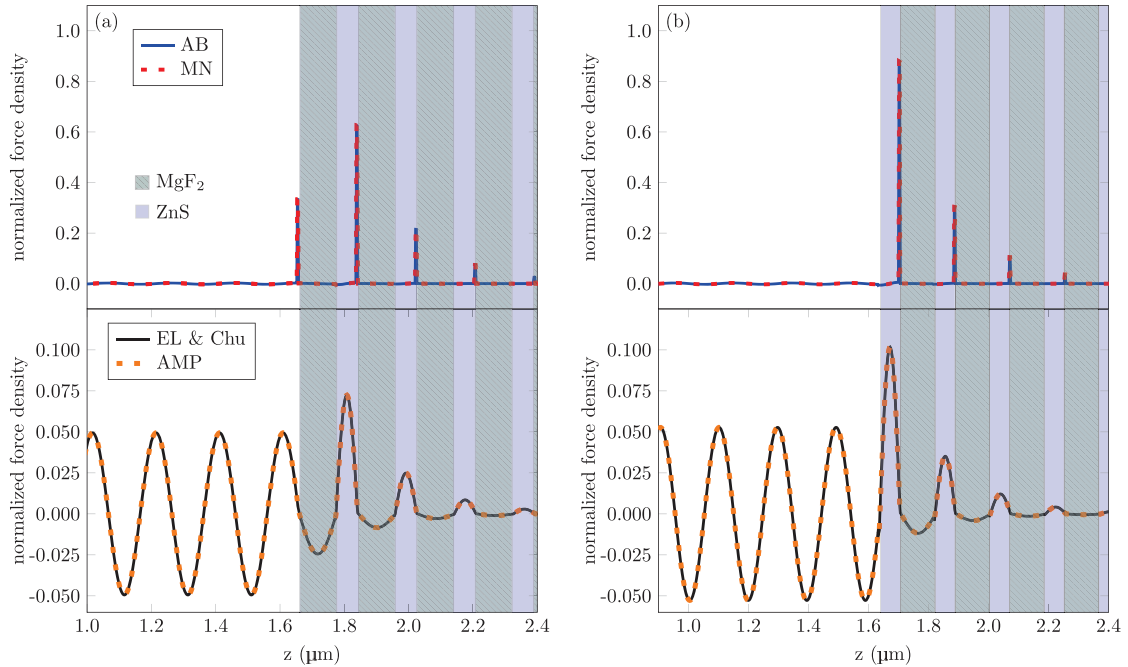


Figure 10. Time-averaged force density distributions predicted by the Minkowski, Abraham, Einstein–Laub, Chu, and Amperian postulates, shown for the case of a continuous-wave beam ($\lambda_0 = 632.8$ nm) normally incident onto a dielectric mirror composed of alternating quarter-wavelength-thick layers of MgF_2 and ZnS submerged in a fluid of refractive index $n = 1.6$. We consider the configuration in which the dielectric mirror is capped by (a) the lower-index layer and (b) the higher-index layer. Degenerate time-averaged force density distributions predicted by (top) the Abraham (solid blue) and Minkowski (dashed red) postulates and (bottom) the Einstein–Laub and Chu postulates (solid black) and the Amperian postulates (dashed orange). The former is dominated by strong surface forces localized at transitions from high to low refractive index regions, whereas the latter is dominated by weaker oscillatory body forces extending across the fluid and mirror regions. All force density distributions have been normalized to the peak instantaneous Abraham force density.

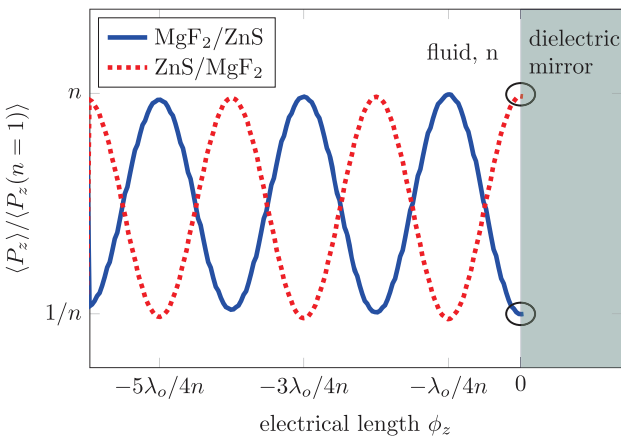


Figure 11. Normalized radiation pressure on a submerged dielectric mirror predicted by the Einstein–Laub, Chu, and Amperian postulates as a function of the force density integration distance into the fluid for cases in which the dielectric mirror is capped by either the lower-index layer (blue solid) or the higher-index layer (red dashed). Here, n represents the refractive index of the surrounding fluid medium. The circles denote the nominal radiation pressure when the force density is integrated up to the boundary of the mirror. The addition of body forces in the fluid causes the normalized radiation pressure to oscillate between an upper bound of n and a lower bound of $1/n$.

for illumination downward from the air or upward from water, was initially interpreted by Ashkin and Dziedzic as evidence of the on-axis recoil associated with the Minkowski form of

light momentum [14]. Subsequently, Gordon [71] proposed an alternative explanation based on compressive lateral radiation forces squeezing the water into the highest-intensity region of the beam, a so-called ‘toothpaste’ effect that forced water to bulge up into the air above. This viewpoint has gained traction [24, 108] but has yet to be proven. Recently, laser-induced deformations of an air–water interface were shown to be accurately modelled without explicitly invoking compressive forces [58, 90]. The model described interface deformation using the Navier–Stokes equation driven by a Minkowski-like on-axis recoil given by equation (19), evidence that suggests a Minkowski form of momentum.

Radiation-induced fluid deformations of much greater effect have been studied by Casner *et al* [15–19]. In place of an air–water interface was a carefully designed liquid–liquid interface, where the composition of the liquids was tuned to achieve a surface tension 10^4 times smaller than that of an air–water interface. Because the higher-index fluid sat atop the lower-index fluid, deformation of the interface towards the lower-index fluid would be directed along, rather than opposed to, gravity. It was shown that illumination of the fluid–fluid interface with even a moderately-powered (≈ 150 mW) continuous-wave 632 nm-wavelength laser beam could cause millimeter-scale downward bulges into the lower-index liquid, irrespectively of the illumination direction [18, 19]. The much larger bulge magnitudes enabled detailed studies of the interface morphology and asymmetric deformations dependent on illumination direction [109]. The similarities

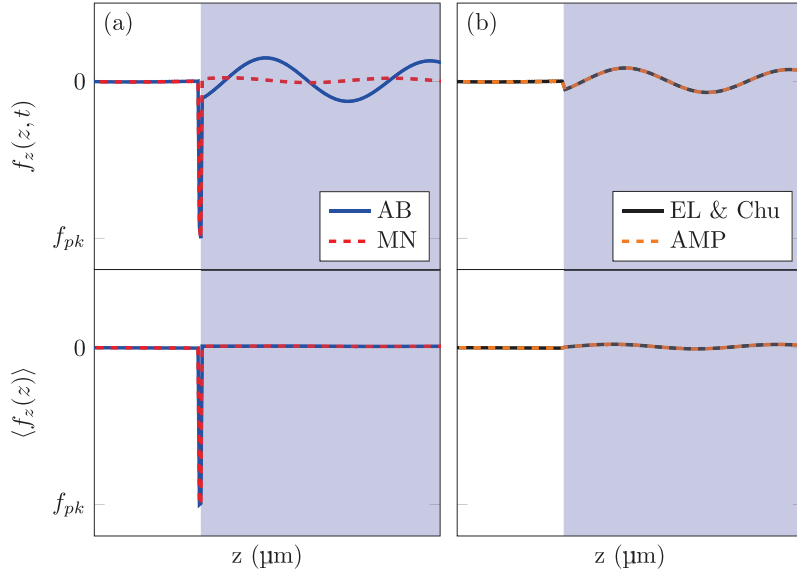


Figure 12. Instantaneous (top row) and time-averaged (bottom row) electromagnetic force density distribution exerted by a continuous-wave beam ($\lambda_0 = 632.8$ nm) normally incident from air onto water ($n = 1.33$) predicted by (a) the Abraham (solid blue) and Minkowski (dashed red) postulates and (b) the Einstein–Laub and Chu postulates (solid black) and the Amperian postulates (dashed orange).

in the light-induced deformations observed for air–water and liquid–liquid interfaces—both deform from high-index to low-index regions—suggest a common physical origin, but a consolidated model rooted in the basic electrodynamic postulates has yet to be proposed. Such efforts, however, are important for resolving the roles of lateral and longitudinal forces and elucidating the link, if any, between fluid deformations and light momentum in matter.

Realistic descriptions of radiation-induced fluid deformation must abandon the assumption of material rigidity, a significant departure from ideality that requires careful re-examination of the nature of recoil. Figure 12 shows snapshots of the instantaneous force density distribution described by all five postulates, for the case of a plane wave impinging at normal incidence onto a dielectric from free space. The force density distributions are characterized by localized surface pressure (Minkowski), undulating body forces (Einstein–Laub, Chu and Amperian), or a combination of both (Abraham). Under the assumption that the medium is rigid, momentary imbalances in the force density distribution extending across the entire medium can result in a net recoil. However, under the realistic assumption that the medium is deformable, such recoil mechanisms are impossible as it requires instantaneous communication of force density across finite extents. Instead, each element of the medium is locally driven by a time-averaged force density, which, as shown in figure 12, can be substantially different from the instantaneous force density. Time-averaging generally diminishes the undulations in the instantaneous force density distributions, so much so for the Abraham force density that it becomes indistinguishable from the Minkowski force density. In this case, models of recoil based on the Minkowski and Abraham time-averaged force densities predict identical backwards recoil driven entirely by surface pressure. This contrasts to classical models of recoil based simply on changes in light momentum

at threshold of a dielectric, which predict opposing recoils for light momentum of Minkowski and Abraham forms [36, 58].

Both electrodynamics and fluid dynamics are needed to completely understand how fluids deform under radiation pressure. Since the time scales of fluid deformation are much greater than the times scales of electromagnetic oscillation (particularly at visible frequencies), the physics of radiation-induced fluid deformation can be captured without solving the electrodynamic and fluid dynamic equations simultaneously. We use a coupled electrodynamic-hydrodynamic simulator in which Maxwell’s equations and the Navier–Stokes equations are solved on respective grids of fine and coarse spatio-temporal resolution. The electrodynamic simulator calculates the time-averaged force density, which is ported to the hydrodynamic simulator to calculate an updated fluid geometry. We examine two configurations: pulsed excitation of an air–water interface like in the Ashkin–Dziedzic experiment [14] and continuous-wave visible excitation of a low-tension fluid–fluid interface like in the experiments by Casner *et al* [18, 19]. To emulate impulsive excitation, we drive the hydrodynamic simulator at a single coarse time step with the time-averaged force density profile calculated for the initial fluid configuration, a valid procedure only because the coarse time step is several orders of magnitude longer than the pulse duration. To emulate continuous-wave excitation, we cyclically compute the time-averaged force density and resulting fluid geometry each time the interface has deformed by at least one coarse space step. The simulations assume a simplified two-dimensional configuration which does not fully describe the tightly focused beams used in the experiments [14, 18, 19], but has a sufficient degree of complexity to illustrate lateral forces associated with electrostriction and field gradients.

Figure 13 illustrates the initial time-average force distribution applied to an impulsively-excited air–water interface and the ensuing interface deformation and fluid velocity. Three

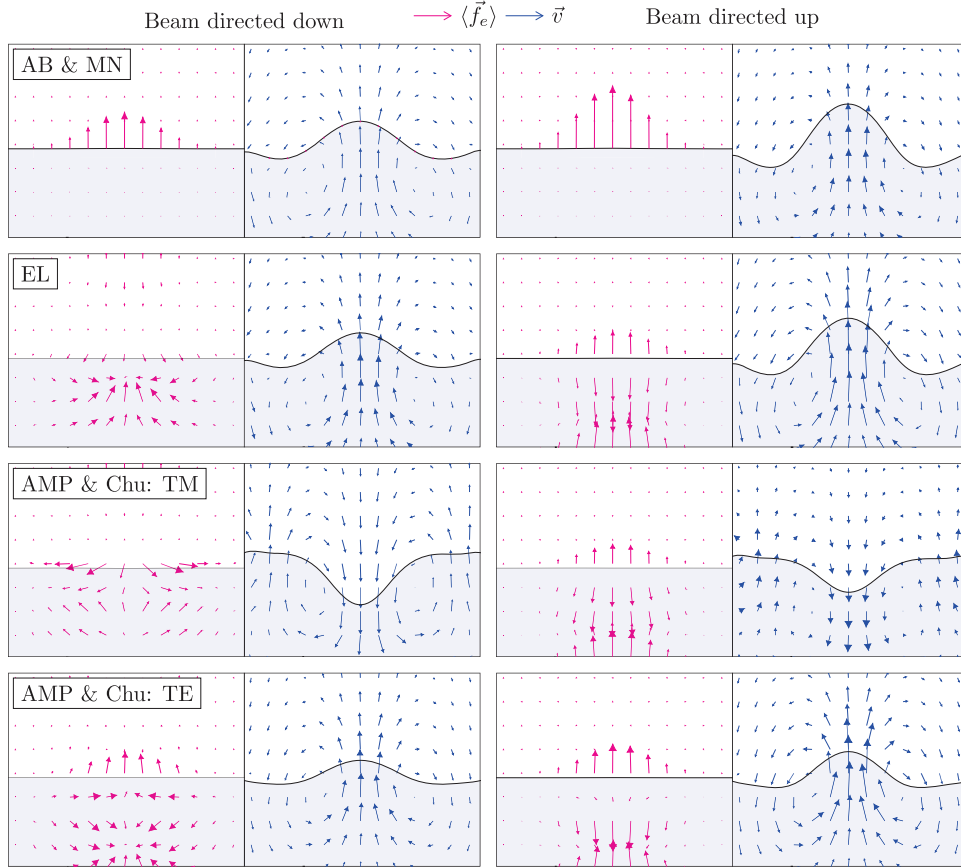


Figure 13. Two-dimensional fluid dynamic simulations representative of the Ashkin–Dziedzic experiment [14]. The lower fluid (blue) represents water ($n = 1.33$) and the upper fluid (white) represents air ($n = 1$). The air–water interface is excited by a 60 ns-long, 530-nm-wavelength pulse at normal incidence. The time-averaged force density distributions exerted by the pulse are calculated using the Minkowski, Abraham, Einstein–Laub, Chu, and Amperian postulates (magenta arrows), which are shown next to the resulting velocity field (blue arrows) of the deformed interface. We set the surface tension of the water-air interface to $\sigma = 0.7 \text{ N m}^{-1}$ and the viscosity of water to $\eta = 1 \text{ mPa}\cdot\text{s}$. The Abraham, Minkowski, and Einstein–Laub postulates predict an upward bulge for TE and TM polarizations for both illumination directions. The Amperian postulates predict an upward and downward bulge for TM and TE polarizations, respectively. Mesh refinement studies have been performed to ensure convergence of the simulated fluid behaviour.

unique sets of bulge dynamics emerge. For both transverse-magnetic (TM) and transverse-electric (TE) polarizations, only the Abraham, Minkowski, and Einstein–Laub postulates predict an upward bulge for illumination from air or water, qualitatively consistent with the results of the Ashkin–Dziedzic experiment [14]. The Amperian and Chu postulates, on the other hand, predict upward bulges for TE polarization, which are smaller than those predicted by the other postulates, and downward bulges for TM polarization. The latter case provides further proof of the empirical invalidity of the Amperian and Chu postulates. This conclusion is consistent with those made by Mansuripur *et al* [57] after comparing the effect imparted by a beam to a dielectric medium using the Einstein–Laub and Lorentz force densities.

The Abraham, Minkowski, and Einstein–Laub postulates offer two physical mechanisms to explain the appearance of an upward bulge: it can arise from a longitudinal upward force density localized at the interface (Minkowski and Abraham) or a lateral compressive force density applied to the bulk of water (Einstein–Laub). The former is consistent with the Minkowski surface recoil described by equation (19), and the latter describes the toothpaste effect suggested by Gordon

[71]. The bulge shape and size resulting from either mechanism are nearly identical and indistinguishable with respect to the precision of the Ashkin–Dziedzic experiment [14], although repetition of the experiment with fluids of different viscosities and mass densities may lead to more diverse bulge shapes that better distinguish surface and body effects. For the Abraham, Minkowski, and Einstein–Laub postulates, illumination from water yields larger bulges than illumination from air, a general consequence of the larger field magnitudes and larger force densities in water when it is used as the incidence region. The interplay between force density distributions and interface deformation can be complex. For example, the Einstein–Laub postulates predict downward body forces when illuminated from water, which are overwhelmed by an upward surface force and overall compressive forces that conspire to generate an upward bulge.

The bulge dynamics observed by Casner *et al* [18, 19] for a fluid–fluid interface have been distinguished by two regimes: a low-power regime in which the bulge sizes are small and scale linearly with power and a high-power regime in which the bulge exhibits large interface instabilities. Recent investigations have suggested that the instabilities in the high-power

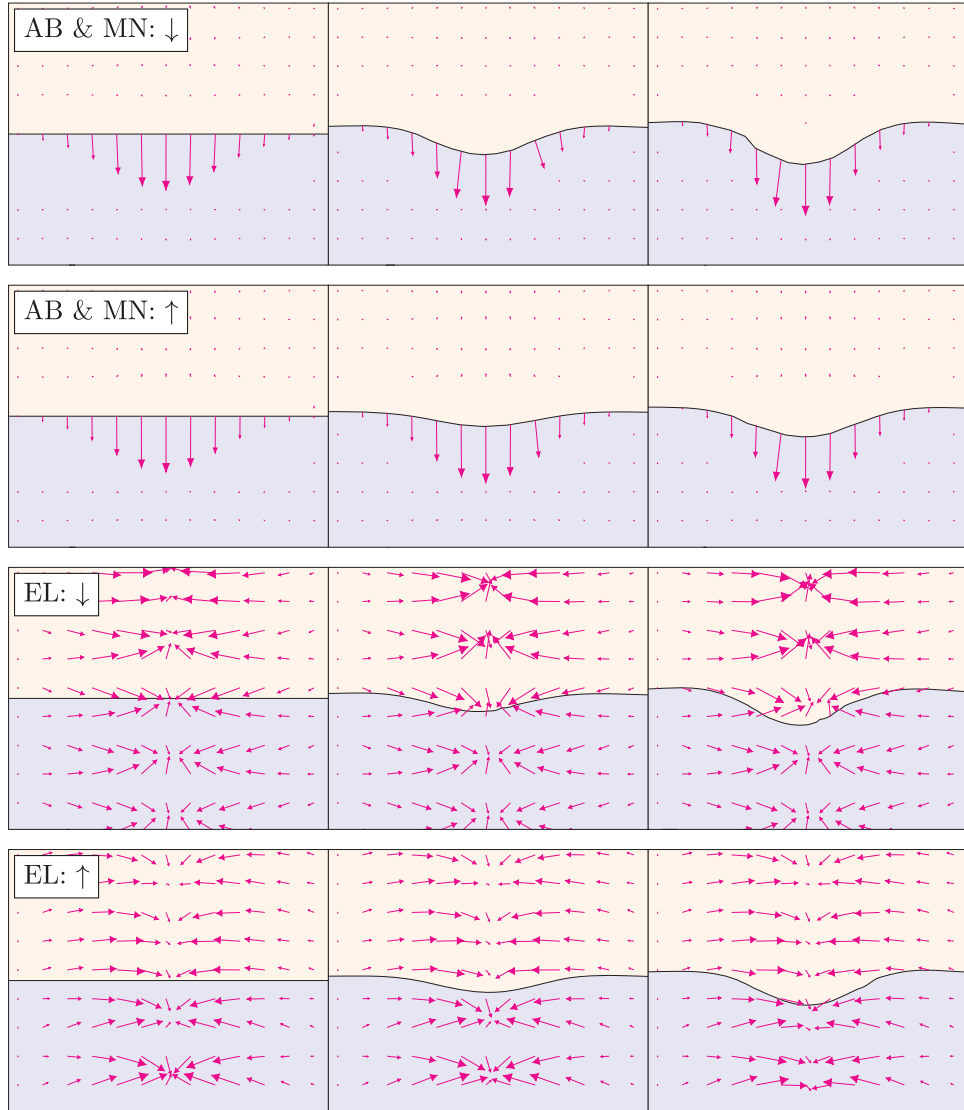


Figure 14. Two-dimensional fluid dynamic simulations representative of the experiments by Casner *et al* [18, 19]. The experiments used a micellar phase of microemulsions made from a liquid mixture of mass composition 9% water, 4% sodium dodecyl sulfate, 70% toluene, and 17% n-butanol. Below the critical temperature of 35 °C, the mixture separates into two phases of different micellar concentrations. The two phases are represented in the simulations as two continuous fluid media in which the upper fluid (beige) has index $n = 1.49$ and mass density $\rho = 853 \text{ kg m}^{-3}$ and the lower fluid (blue) has index $n = 1.46$ and mass density $\rho = 1017 \text{ kg m}^{-3}$ [137]. Near the critical temperature, the fluids have the same viscosity of $\eta = 1.3 \text{ mPa}\cdot\text{s}$ and an extremely low surface tension of $0.1 \mu\text{N m}^{-1}$. The fluid mixture is excited by a continuous-wave TM-polarized beam ($\lambda_0 = 532 \text{ nm}$) with a Gaussian profile. The time-averaged electromagnetic force density distributions (magenta arrows) calculated using the Minkowski, Abraham, and Einstein–Laub postulates for downward (\downarrow) and upward (\uparrow) illumination are shown for three instances during the evolution of a radiation-pressure-driven surface bulge. The three postulates all predict downward bulge formation from the high-index region into the low-index region, consistent with the observations by Casner *et al* [137]. Mesh refinement studies have been performed to ensure convergence of the simulated fluid behaviour.

regime are likely caused by surface heating [109], which cannot be treated by our simulations. We therefore restrict our analysis to the low-power regime. Figure 14 shows two sets of simulated bulge and force distribution dynamics: one predicted by the Abraham or Minkowski postulates and the other by the Einstein–Laub postulates. The bulge dynamics of the fluid–fluid interface are consistent with the dynamics of the air–water interface, but reversed in direction since the optically denser region now resides above the interface. The downward bulge for both illumination directions and the slightly larger bulge sizes for downward illumination are both consistent with observations [18, 19]. The bulge can originate

from a downward surface pressure (Minkowski and Abraham) or a pinching effect distributed throughout the bulk (Einstein–Laub). With all things equal, bulges due to surface pressure exhibit larger asymmetries with respect to illumination direction, a feature potentially useful for empirical validation of the two mechanisms of bulge formation.

4.4. Optical tweezers and tractor beaming

The most common application of radiation pressure is the use of finite-sized light beams for dexterous, non-contact manipulation of small objects in low-friction environments. Beam

action on objects can be heuristically understood to arise from a combination of gradient forces, which tend to drag an object towards the highest-intensity part of the beam, and scattering forces, which tend to push an object along the direction of beam propagation. Experimental studies of these interactions offer a wealth of evidence for validation of different electrodynamic theories, but fundamental interpretations have been limited and based on just a few electrodynamic postulates [45, 89, 110–112]. Here, we re-visit experiments of both types using multiple formulations of electrodynamics.

Optical tweezers use gradient forces of a focused light beam to draw a dielectric particle towards the beam center in the lateral directions [113]. For sufficiently strong focusing, the gradient forces along the beam axis can overcome forward scattering forces to trap a particle in all three dimensions [114–116]. A complete theory of optical tweezers has yet to be developed [54, 116] and progression towards this goal will rely on the resolution of electrodynamic controversies. Nevertheless, constrained theoretical descriptions have been made under simplifying approximations and, in some cases, with the use of selective postulates. For dielectric particles much larger than the wavelength, the trapping forces exerted by optical tweezers can be understood by the deflection of optical rays, which do not require knowledge of the light momentum inside the particles [117]. For dielectric particles that are comparable to and smaller than the wavelength, models of optical tweezers require electromagnetic force calculation that must invoke some electrodynamic postulates. Barton *et al* [111] pioneered the approach of using Mie theory to express the fields incident on and scattered from a spherical particle in expanded form and then using the electromagnetic stress tensor to calculate the force on the particle. The original expressions derived by this approach [111] used the Minkowski form of the stress tensor, whose correctness over other forms of stress tensor was assumed a priori on the basis of earlier reviews [24, 26]. Although generally accurate for spherical particles having diameters smaller than the wavelength, the applicability of this approach is restricted by its inability to describe realistic incident field distributions, which has been cited as a factor in its discrepancy with experimental measurements [118, 119]. Rohrbach and Stelzer [89] used a more general approach to determine trapping forces on small, sub-wavelength-sized particles by arbitrary beams using a ‘two-component’ approach in which the Lorentz force density was sub-divided into contributions due to field gradients and scattering. This method was validated by consistency between measured and calculated stiffness values for optically-trapped dielectric spheres of sub-wavelength dimensions [110].

The tell-tale characteristics of optical tweezers can be used to benchmark different electrodynamic postulates. Kemp [45] applied analytical solutions of the two-dimensional field scattered by dielectric cylinders using the Minkowski force density to show qualitative accord with Ashkin’s observations of optical trapping [113]. Pfeifer *et al* [120] have argued on the basis of electrodynamic degeneracy that Minkowski and Abraham postulates describe optical tweezers equivalently, differing only with respect to ease of implementation. This seems to contradict calculations by Mansuripur *et al* [57] of

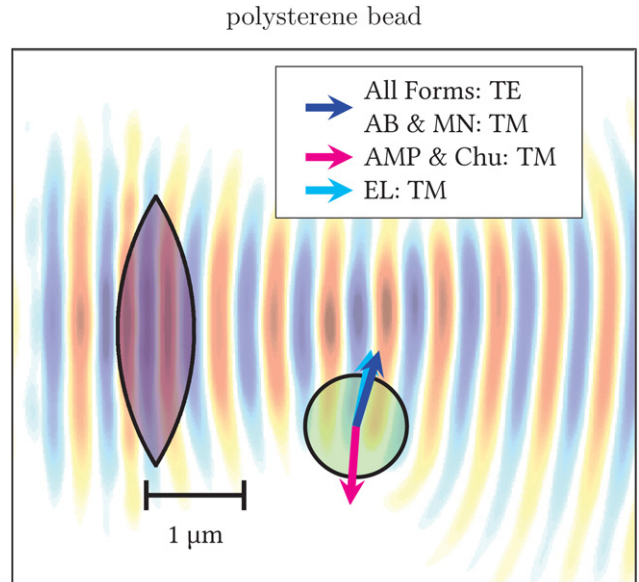


Figure 15. Simulated radiation pressure on a polystyrene bead ($n = 1.58$) placed at the edge of the focal point of a continuous-wave beam ($\lambda_0 = 532$ nm) in a background medium of water ($n = 1.33$). The polystyrene bead ($n = 1.58$) has a diameter of 820 nm and the force acting on it has been determined under the rigid body assumption by integrating the force density distribution within the bead calculated using the Minkowski (MN), Abraham (AB), Einstein–Laub (EL), Chu, and Amperian (AMP) postulates. The bead is shown immersed in a background electromagnetic field calculated using the FDTD method.

the force density within illuminated dielectric particles, which suggest that various postulates can be distinguished by disparities in their distributions of force density. To explore how different postulates describe optical tweezer effects, figure 15(a) depicts simulations that use all five postulates to model the interaction between a focused continuous-wave laser beam with a small, submerged dielectric cylinder placed at the edge of the beam’s focus. For both TM and TE polarizations, only the Minkowski, Abraham, and Einstein–Laub postulates predict effects that are consistent with optical trapping: the focused beam exerts a time-averaged force that drags the particle into the focus and pushes it along the direction of beam propagation. The Amperian and Chu postulates, on the other hand, predict particle trapping for TE polarization and particle expulsion for TM polarization. Forces predicted by the Einstein–Laub postulates also exhibit polarization sensitivity, but to a much lesser extent. This is due to the presence of time-averaged force densities (as seen in previous examples) whose distribution relies on polarization-dependent interference effects inside the particle.

Experiments by Ashkin [113] have shown that air bubbles near a focused beam are repelled from the focus and pushed along the direction of beam propagation. The underlying mechanism of this effect is more complicated than optical tweezer effects on dielectric particles. Whereas the actuation of a dielectric particle is driven by optical forces acting on or within the particle, the actuation of an air bubble is driven by optical forces acting on the fluid region surrounding the bubble. We simulate the dynamics of an air bubble near a focused

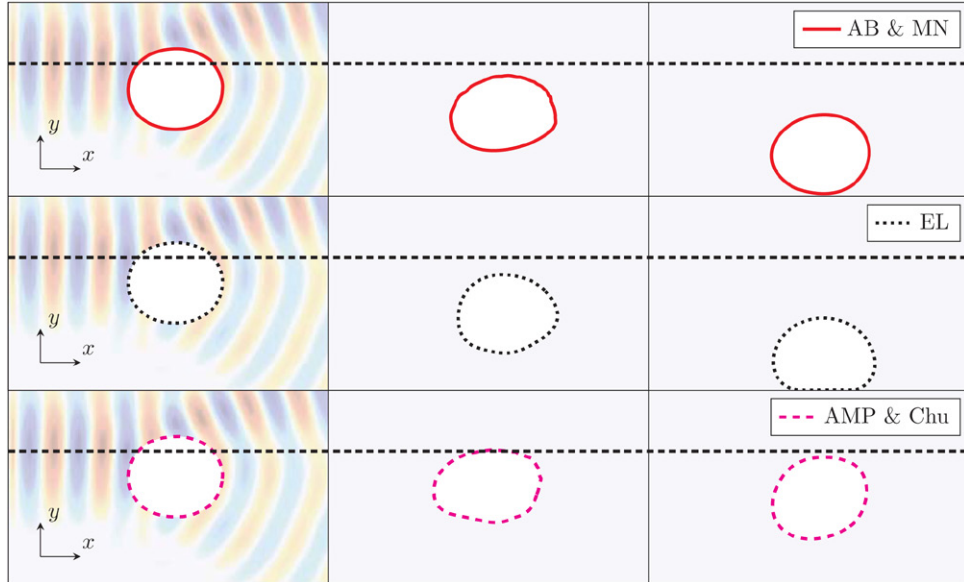


Figure 16. Simulated dynamics of an air bubble placed at the edge of the focal point of a TM-polarized, continuous-wave beam ($\lambda_0 = 532$ nm) in a background medium of water ($n = 1.33$, $\sigma = 0.7 \text{ N m}^{-1}$, $\eta = 1 \text{ mPa}\cdot\text{s}$). The air bubble ($n = 1.00$) has a diameter of 820 nm. The evolution of the deformable bubble in a background electromagnetic field is modelled in two-dimensions by solving both electrodynamic and fluid dynamic equations. The simulated bubble dynamics predicted by (top row) the Minkowski and Abraham postulates, (center row) the Einstein–Laub postulates, and (bottom row) the Chu and Amperian postulates. The dashed horizontal line indicates the axis of the focused beam. In all cases, the bubble is pushed away from the beam axis and along the direction of beam propagation, albeit with different bubble shapes and trajectories. Overall, the simulated behaviour using all postulates is qualitatively consistent with observations by Ashkin [113].

beam using the electrodynamic-hydrodynamic simulator. As shown in figure 16, the five postulates all predict that the air bubble is displaced away from the beam focus and along the direction of beam propagation, which is qualitatively consistent with past observations by Ashkin [113]. Predictions of bubble expulsion differ in terms of rate, shape, and trajectory. Similar to previous examples, the five postulates applied to the case of TM polarization yield three unique sets of dynamics: one degenerate for Abraham and Minkowski postulates, another for the Einstein–Laub postulates, and a third degenerate for Amperian and Chu postulates. With all things equal, lateral bubble expulsion is predicted to be fastest for the Einstein–Laub postulates and slowest for the Amperian and Chu postulates, discrepancies which can potentially be validated by measurements.

In recent years, there has been increased interest in using light beams to ‘pull’ on a particle such that the projection of its displacement onto the incident beam direction has a negative sign. This has been colloquially referred to as ‘tractor beaming’ [112, 121–127]. Theoretical proposals to realize tractor beaming have been put forward based on interfering beams with longitudinal components [122], tailored plane waves [123], or a single non-paraxial Bessel beam [124, 125]. Experimental demonstration of tractor beaming has been realized using two types of forces: non-conservative gradient forces based on a solenoidal beam [128] or pairs of co-axial Bessel beams [126] and conservative scattering forces based on beam-object configurations that achieve enhanced forward-light scattering [112, 127]. It has been suggested that the latter provides direct hints of the light momentum in matter. For example, Kajorndejnukul *et al* [112] showed that oil droplets

confined at the interface of air and water can be pulled along the interface and into the direction of a lightly focused beam obliquely incident onto the droplets from the air region. This observation was interpreted to arise from an increase in the forward light momentum inside the droplet, propelling the droplet in the backward direction. Since the refractive index of the droplet is higher than that of air or water, an increase of light momentum in the droplet was attributed to a Minkowski form of momentum. Simulations of these experiments suggest that alternative explanations are feasible. As shown in figure 17, the Minkowski, Abraham, and Einstein–Laub postulates all predict that an oil droplet resting at the interface of air and water can be pulled into the direction of an obliquely incident laser beam, despite differences in how they predict light momentum to scale with refractive index. The Amperian and Chu postulates, on the other hand, predict a push. In another example of tractor beaming, Brzobohatý *et al* [127] showed that two obliquely-incident plane waves can exert pulling forces on a dielectric particle placed in the region of interference. This observation was modelled using the theory of optical tweezers developed by Barton *et al* [111] based on the Minkowski stress tensor. Figures 18(a) and (b) shows simulations of a dielectric particle illuminated by two obliquely incident plane waves that work together to pull on the particle. Due to the highly symmetric illumination conditions that establish standing waves in the vicinity of the particle, all five postulates make identical force predictions for both polarizations. As shown in figure 18(c), the angle- and polarization-dependence of the normalized lateral force match the results from calculations presented in [127], all of which indicate a tractor-beaming effect for TE polarization and at steep angles

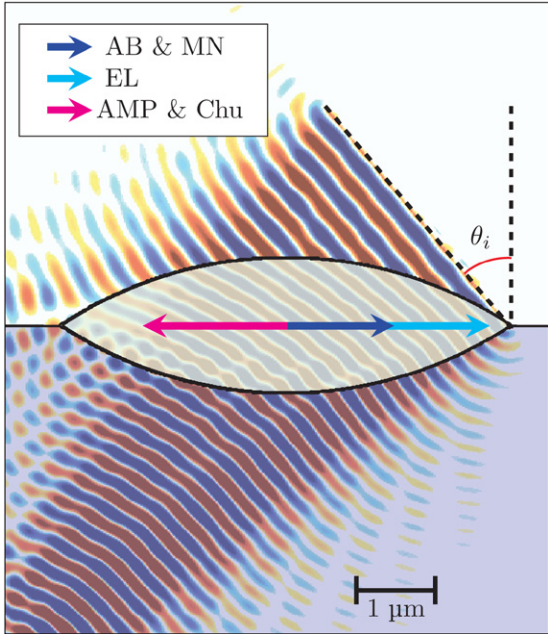


Figure 17. Tractor beaming of an oil droplet ($n = 1.42$) resting at the interface between air ($n = 1.0$) and water ($n = 1.33$). The length, height, and radius of curvature of the droplet are $6.4 \mu\text{m}$, $2 \mu\text{m}$, and $6 \mu\text{m}$, respectively, which are comparable to the dimensions of the droplets studied in [123]. A TM-polarized plane-wave ($\lambda_0 = 532 \text{ nm}$) is incident onto the droplet at an angle of incidence $\theta_i = 50^\circ$. Resulting forces predicted by the Minkowski and Abraham postulates (blue arrow), the Einstein–Laub postulates (dashed black arrow), and the Amperian and Chu postulates (magenta arrow). The reflected fields bouncing off the droplet and propagating behind the diagonal source line have been removed for clarity.

of incidence. Thus, recent studies of tractor beaming do not offer sufficiently discerning experimental proof to pin down a single electrodynamic theory.

4.5. Conclusion

Radiation pressure is the observable manifestation of an intricate system of interactions between electromagnetic waves and material bodies. A complete mathematical description of these interactions, first presented in the broad context of basic conservation principles by Penfield and Haus [10], requires postulated definitions of electromagnetic momentum, stress, force, energy, and power. Conservation principles alone, however, are insufficient to pin down a unique combination of electrodynamic postulates, the root cause of the diverse formulations presented to date [26, 40, 45]. Hopes to validate a single formulation must instead rely on empirical validation against observable phenomena. To this end, we have re-visited the most important studies of radiation pressure from the perspective of five historically significant sets of postulates. Detailed predictions of radiation pressure have been generated in a simulation test-bed that uses the sub-system concept of Penfield and Haus [10] to completely and consistently describe energy and momentum exchange between an electrodynamic sub-system composed of fields and a kinetic sub-system composed of matter. The electrodynamic sub-system

is governed by Maxwell's equations and any one of the five sets of electrodynamic postulates, and the kinetic sub-system is governed by Newtonian dynamics applied to either rigid or deformable bodies. Economy in assumptions and generality in implementation have enabled the virtual replication of past experiments to a high degree of similitude.

We have reviewed four historically significant ways to probe light momentum: considerations of center-of-mass translation akin to the thought experiment presented by Balazs [37], radiation pressure measurements on mirrors made by Jones–Richards [12] and Jones–Leslie [13], observations of radiation-induced deformation of fluid interfaces [14–19], and manipulation of small dielectric particles by focused laser beams [112, 113, 127]. Although postulates can be degenerate in some scenarios, over the diverse range of conditions explored, each postulate has made a unique set of predictions about how matter deforms under light action. This offers strong evidence against the hypothesis that the various electrodynamic theories are completely degenerate and the use of any particular theory is a matter of personal choice.

Predictions made by the five postulates have been compared with observations and other fundamental laws and withstood the comparison to varying degrees of success. Although the Minkowski and Abraham postulates make similarly accurate predictions of radiation pressure phenomena and can both be made consistent with conservation laws, the advantage goes to the Abraham postulates due to its more plausible description of power flow that does not require hidden energy concepts. The Einstein–Laub, Chu, and Amperian postulates make identical predictions of radiation pressure on submerged mirrors, but only the Einstein–Laub postulates are capable of accurately modelling radiation pressure on fluid interfaces and small objects. Overall, out of the five postulates, the Abraham and Einstein–Laub postulates offer the most physically reasonable and experimentally satisfactory accounts of radiation pressure and light momentum in all configurations. Both postulate sets invoke the Abraham momentum density and, thus, the analysis endorses the Abraham side of the Abraham–Minkowski debate. However, the momentum density is just one part of a still-incomplete picture of light-matter interaction that must also call into question the densities of energy, power, force, and stress in matter. Interestingly, the Abraham and Einstein–Laub postulates make distinct predictions of electromagnetic force density. We have shown that the radiation pressure on submerged mirrors is phase dependent for the Einstein–Laub postulates but not the Abraham postulates. In addition, laser-induced bulges on fluid surfaces predicted by the Abraham postulates are driven by surface pressure, whereas those predicted by the Einstein–Laub postulates are driven by bulk forces akin to the toothpaste effect. In optical tweezer experiments, the forces predicted by the Abraham and Einstein–Laub postulates are similar in magnitude and direction, but the latter can be distinguished by its polarization dependence.

Simulations of radiation pressure dynamics challenge well-established views forged long ago by various inferential deductions and approximate analytical expressions. (1) Contrary to the result of the original Balazs thought experiment,

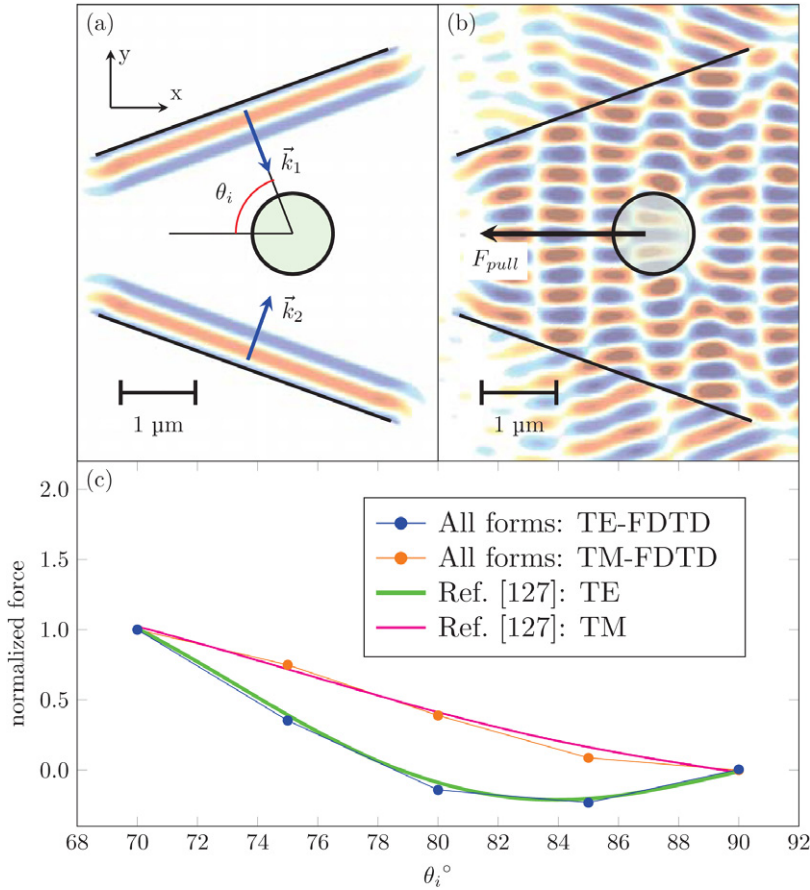


Figure 18. Tractor beaming of a dielectric particle using two obliquely incident plane waves. Simulation snapshots of two TE-polarized plane waves ($\lambda_0 = 532$ nm) incident at $\theta_i = 70^\circ$ onto a polystyrene cylinder ($d = 820$ nm, $n = 1.58$) immersed in water ($n = 1.33$), shown (a) before the plane waves strike the bead and (b) at steady state when the plane waves collide to exert a pulling force in the $-x$ direction. (c) Force on the bead calculated by FDTD using the Minkowski, Abraham, Einstein–Laub, Chu, and Amperian postulates for both TE (blue circles) and TM (orange circles) polarizations as a function of incident angle θ_i . The forces have been normalized to the force magnitude at $\theta_i = 70^\circ$. Under the highly symmetric illumination conditions studied here, all five postulates make degenerate force predictions. Pulling forces are only achieved for TE polarization within the range $76^\circ < \theta_i < 90^\circ$. Excellent agreement is observed with the three-dimensional Mie-theory calculations (solid lines) by Brzobohatý *et al* [127], despite the reduced dimensionality of the simulations.

center-of-mass velocity in a closed system containing fields and matter can be conserved using all five postulates, including those that endorse a momentum density other than Abraham's. For example, the Minkowski momentum density $\vec{D} \times \vec{B}$ can be made to conserve center-of-mass velocity provided that power flux density is defined as $c^2 \vec{D} \times \vec{B}$, in accordance with mass-energy equivalence. However, use of power flux definitions different from the canonical Poynting vector results in the necessary presence of surface energy densities that must be reconciled by notions of hidden energy. (2) Previous radiation pressure measurements on submerged mirrors do not provide conclusive proof of a particular electrodynamical theory, largely because experimental details necessary for rigorous comparison to theory are missing from the original reports. For example, simulations of the Jones–Richards experiment yield different radiation pressure curves depending on whether the rhodium-coated silver mirror is modelled as rhodium, silver, or a combination of both. Similarly, simulations of the Jones–Leslie experiment using some postulates can vary significantly depending on the specific ordering of the layers. Immediate future work should focus on detailed radiation pressure measurements on well-characterized reflective mirrors of either

metallic or dielectric composition. (3) Contrary to the widely held belief that radiation-induced bulges on fluid interfaces are supportive of the Minkowski postulates [14, 18, 129], we have shown that they can be explained equally well using the Abraham, Minkowski, and Einstein–Laub postulates. Both longitudinal recoil and lateral compression offer physically plausible explanations of observed bulge shapes and can be distinguished based on asymmetries with respect to illumination direction. (4) Optical tweezers and tractor beaming effects, both commonly described using Minkowski postulates (and thus argued to support the Minkowski momentum density), can also be described using the Abraham and Einstein–Laub postulates.

A limitation of our analysis is that it does not incorporate thermodynamic models describing the transformation of electromagnetic energy into heat, precluding realistic description of material deformation due to thermal expansion. This limitation is justifiable only within the scope of our selected experimental case studies, which have all exercised care in mitigating heating effects, for example, by using low-loss dielectric materials and force-sensitive systems with high mechanical compliance.

Strides have thus been taken towards a true electrodynamic theory, but future work remains. Experimental tests to distinguish the theories of Abraham and Einstein–Laub could involve measurements of radiation pressure on submerged mirrors (especially dielectric mirrors with different layer ordering) and non-equilibrium dynamics of illuminated fluid surfaces and small objects. Electrodynamic postulates defined using the magnetic field or magnetic flux density can be verified by radiation pressure measurements on magnetic materials, which have received little attention outside of a few experiments in the microwave regime [130–133]. The advent of metamaterials, engineered composites designed to have counter-intuitive properties, also raises new and interesting questions about the form of momentum and energy in highly complex structures [32, 73, 88, 134–136], which can be probed using a combination of simulation predictions and experimental validation. It is believed that these suggested studies, and more, will ultimately form an aggregate picture of light-matter interaction that should be cohesively bound by a single theory of electrodynamics.

Acknowledgments

This work was supported by the Natural Sciences and Engineering Research Council of Canada (NSERC): Discovery Grant 366136. The authors acknowledge helpful discussions with Dr T Johnson from The University of British Columbia.

References

- [1] Maxwell J C 1891 *A Treatise on Electricity and Magnetism* vol 2 (New York: Dover)
- [2] Lebedev P N 1900 Untersuchungen über die Druckkräfte des Lichtes *Ann. Phys.* **6** 433–58
- [3] Nichols E F and Hull G F 1901 A preliminary communication on the pressure of heat and light radiation *Phys. Rev.* **13** 307–20
- [4] Nichols E F and Hull G F 1903 The pressure due to radiation (Second Paper) *Phys. Rev.* **17** 26–50
- [5] Minkowski H 1908 Die Grundgleichungen für die elektromagnetischen Vorgänge in bewegten Körpern *Nachr. Ges. Wiss. Göttingen* **1908** 53–111
- [6] Abraham M 1909 Zur Elektrodynamik bewegter Körper *Rend. Circ. Mat. Palermo* **28** 1–28
- [7] Einstein A and Laub J 1908 Über die elektromagnetischen Grundgleichungen für bewegte Körper *Ann. Phys.* **26** 541–50
Beck A 1989 *The Collected Papers of Albert Einstein* (Princeton: Princeton University Press) pp 329–48
- [8] Fano R M, Chu L J and Adler R B 1960 *Electromagnetic Fields, Energy, and Forces* (New York: Wiley)
- [9] Chu L J, Haus H A and Penfield P Jr 1966 The force density in polarizable and magnetizable fluids *Proc. IEEE* **54** 920–35
- [10] Penfield P and Haus H A 1967 *Electrodynamics of Moving Media* (Cambridge: MIT Press)
- [11] Obukhov Y N and Hehl F W 2003 Electromagnetic energy-momentum and forces in matter *Phys. Lett. A* **311** 277–84
- [12] Jones R V and Richards J C S 1954 The pressure of radiation in a refracting medium *Proc. R. Soc. Lond.* **221** 480–98
- [13] Jones R V and Leslie B 1978 The measurement of optical radiation pressure in dispersive media *Proc. R. Soc. Lond. A* **360** 347–63
- [14] Ashkin A and Dziedzic J M 1973 Radiation pressure on a free liquid surface *Phys. Rev. Lett.* **30** 139–42
- [15] Casner A and Delville J-P 2001 Giant deformations of a liquid–liquid interface induced by the optical radiation pressure *Phys. Rev. Lett.* **87** 054503
- [16] Casner A, Delville J-P and Brevik I 2003 Asymmetric optical radiation pressure effects on liquid interfaces under intense illumination *J. Opt. Soc. Am. B* **20** 2355–62
- [17] Casner A and Delville J-P 2003 Laser-induced hydrodynamic instability of fluid interfaces *Phys. Rev. Lett.* **90** 144503
- [18] Wunenburger R, Casner A and Delville J-P 2006 Light-induced deformation and instability of a liquid interface. I. Statics *Phys. Rev. E* **73** 036314
- [19] Wunenburger R, Casner A and Delville J-P 2006 Light-induced deformation and instability of a liquid interface. II. Dynamics *Phys. Rev. E* **73** 036315
- [20] Gibson A F, Kimmitt M F and Walker A C 1970 Photon drag in germanium *Appl. Phys. Lett.* **17** 75–7
- [21] Danishevskii A M, Kastal'skii A A, Ryvkin S M and Yaroshetskii I D 1970 Dragging of free carriers by photons in direct interband transitions in semiconductors *Sov. Phys.—JETP* **31** 292–5
- [22] Gibson A F, Kimmitt M F, Koohian A O, Evans D E and Levy G F D 1980 A study of radiation pressure in a refractive medium by the photon drag effect *Proc. R. Soc. Lond. A* **370** 303–11
- [23] Campbell G K, Leanhardt A E, Mun J, Boyd M, Streed E W, Ketterle W and Pritchard D E 2005 Photon recoil momentum in dispersive media *Phys. Rev. Lett.* **94** 170403
- [24] Robinson F N H 1975 Electromagnetic stress and momentum in matter *Phys. Rep.* **16** 313–54
- [25] Mikura Z 1976 Variational formulation of the electrodynamics of fluids and its application to the radiation pressure problem *Phys. Rev. A* **13** 2265–75
- [26] Brevik I 1979 Experiments in phenomenological electrodynamics and the electromagnetic energy-momentum tensor *Phys. Rep.* **52** 133–201
- [27] Kemp B A and Grzegorczyk T M 2011 The observable pressure of light in dielectric fluids *Opt. Lett.* **36** 493–5
- [28] Milonni P W and Boyd W 2005 Recoil and photon momentum in a dielectric *Laser Phys.* **15** 1432–8
- [29] Barnett S M 2010 Resolution of the Abraham–Minkowski dilemma *Phys. Rev. Lett.* **104** 070401
- [30] Barnett S M and Loudon R 2010 The enigma of optical momentum in a medium *Phil. Trans. R. Soc. A* **368** 927–39
- [31] Bradshaw D H, Shi Z, Boyd R W and Milonni P W 2010 Electromagnetic momenta and forces in dispersive dielectric media *Opt. Commun.* **283** 650–6
- [32] Mansuripur M and Zakharian A R 2012 Radiation pressure on a submerged absorptive partial reflector deduced from the doppler shift *Phys. Rev. A* **86** 013841
- [33] Poynting J H 1884 On the transfer of energy in the electromagnetic field *Phil. Trans. R. Soc.* **175** 343–61
- [34] Haus H A 1969 Momentum, energy, and power densities of TEM wave packet *Physica* **43** 77–91
- [35] Shockley W 1967 ‘Hidden linear momentum’ related to the $\vec{\alpha} \cdot \vec{E}$ term for a dirac-electron wave packet in an electric field *Phys. Rev. Lett.* **20** 343–6
- [36] Burt M G and Peierls R 1973 The momentum of a light wave in a refracting medium *Proc. R. Soc. Lond. A* **333** 149–56
- [37] Balazs N L 1953 The energy-momentum tensor of the electromagnetic field inside matter *Phys. Rev.* **91** 408–11
- [38] Einstein A 1906 Das Prinzip von der Erhaltung der Schwerpunktsbewegung und die Trägheit der Energie *Ann. Phys.* **20** 627–33

- Beck A 1989 *The Collected Papers of Albert Einstein* (Princeton: Princeton University Press) pp 200–6
- [39] Kranys M 1979 About the equivalence of Abraham's and Minkowski's electrodynamics *Can. J. Phys.* **57** 1022–6
- [40] Pfeifer R N C, Nieminen T A, Heckenberg N R and Rubinsztein-Dunlop H 2007 Momentum of an electromagnetic wave in dielectric media *Rev. Mod. Phys.* **79** 1197–216
- [41] Nelson D F 1991 Momentum, pseudomomentum, and wave momentum: Toward resolving the Minkowski–Abraham controversy *Phys. Rev. A* **44** 3985–96
- [42] Hinds E A and Barnett S M 2009 Momentum exchange between light and a single atom: Abraham or Minkowski? *Phys. Rev. Lett.* **102** 050403
- [43] Milonni P W and Boyd R W 2010 Momentum of light in a dielectric medium *Adv. Opt. Photonics* **2** 519–53
- [44] Baxter C and Loudon R 2010 Radiation pressure and the photon momentum in dielectrics *J. Mod. Opt.* **57** 830–42
- [45] Kemp B A 2011 Resolution of the Abraham–Minkowski debate: Implications for the electromagnetic wave theory of light in matter *J. Appl. Phys.* **109** 111101
- [46] Jones R V 1978 Radiation pressure of light in a dispersive medium *Proc. R. Soc. Lond. A* **360** 365–71
- [47] Peierls R 1976 The momentum of light in a refracting medium *Proc. R. Soc. Lond. A* **347** 475–91
- [48] Mansuripur M 2004 Radiation pressure and the linear momentum of the electromagnetic field *Opt. Express* **12** 5375–401
- [49] Mansuripur M 2005 Radiation pressure and the linear momentum of light in dispersive dielectric media *Opt. Express* **13** 2245–50
- [50] Mansuripur M, Zakharian A R and Moloney J V 2005 Radiation pressure on a dielectric wedge *Opt. Express* **13** 2064–74
- [51] Garrison J C and Chiao R Y 2004 Canonical and kinetic forms of the electromagnetic momentum in an ad hoc quantization scheme for a dispersive dielectric *Phys. Rev. A* **70** 053826
- [52] Saldanha P L 2011 Division of the momentum of electromagnetic waves in linear media into electromagnetic and material parts *Opt. Express* **18** 2258–68
- [53] Brevik I and Ellingsen S Å 2011 Electromagnetic momentum conservation in media *Ann. Phys.* **326** 754–69
- [54] Mansuripur M 2013 Momentum exchange effect *Nat. Photonics* **7** 765–6
- [55] Chau K J and Lezec H J 2012 Revisiting the Balazs thought experiment in the case of a left-handed material: electromagnetic-pulse-induced displacement of a dispersive, dissipative negative-index slab *Opt. Express* **20** 10138–62
- [56] Frias W and Smolyakov A I 2012 Electromagnetic forces and internal stresses in dielectric media *Phys. Rev. E* **85** 046606
- [57] Mansuripur M, Zakharian A R and Wright E M 2013 Electromagnetic-force distribution inside matter *Phys. Rev. A* **88** 023826
- [58] Astrath N G C, Lukasievicz G V B, Malacarne L C and Bialkowski S E 2013 Surface deformation effects induced by radiation pressure and electrostriction forces in dielectric solids *Appl. Phys. Lett.* **102** 231903
- [59] Poincaré H 1900 The theory of Lorentz and the principle of reaction *Arch. Néerlandaises Sci. Exactes Naturelles* **5** 252–78
- [60] Einstein A 1905 Ist die Trägheit eines Körpers von seinem Energieinhalt abhängig? *Ann. Phys.* **18** 639–41
- Beck A 1989 *The Collected Papers of Albert Einstein* (Princeton: Princeton University Press) pp 172–4 (Engl. Transl.)
- [61] Shockley W A 1968 ‘Try Simplest Cases’ resolution of the Abraham–Minkowski controversy on electromagnetic momentum in matter *Proc. Natl Acad. Sci.* **60** 807–13
- [62] Mansuripur M 2014 The Lorentz force law and its connections to hidden momentum, the Einstein–Laub Force, and the Aharonov–Casher effect *IEEE Tran. Magn.* **50** 1300110
- [63] Stratton J A 1941 *Electromagnetic Theory* (New York: McGraw-Hill)
- [64] Griffiths D J 1999 *Introduction to Electrodynamics* 3rd edn (Upper Saddle River, NJ: Prentice Hall)
- [65] Stallinga S 2006 Energy and momentum of light in dielectric media *Phys. Rev. E* **73** 026606
- [66] Griffiths D J 2012 Resource letter EM-1: electromagnetic momentum *Am. J. Phys.* **80** 7–18
- [67] Ives H E 1952 Derivation of the mass-energy relation *J. Opt. Soc. Am.* **42** 540–3
- [68] Planck M 1908 Zur Dynamik bewegter Systeme *Ann. Phys.* **331** 1–34
- [69] Planck M 1908 Bemerkungen zum Prinzip der Aktion und Reaktion in der allgemeinen Dynamik *Phys. Z.* **9** 828–30
- [70] Abraham M 1914 Zur Frage der Symmetrie des elektronegnetischen Spannungstensors *Annal. Phys.* **349** 537–44
- [71] Gordon J P 1973 Radiation forces and momenta in dielectric *Phys. Rev. A* **8** 14–21
- [72] Jackson J D 1999 *Classical Electrodynamics* 3rd edn (New York: Wiley)
- [73] Veselago V G 2009 Energy, linear momentum, and mass transfer by an electromagnetic wave in a negative-refraction medium *Phys.—Usp.* **52** 649–54
- [74] Makarov V P and Rukhadze A A 2011 Negative group velocity electromagnetic waves and the energy-momentum tensor *Phys.—Usp.* **54** 1357–68
- [75] Vorobyev O B 2015 Continuity equation for momentum of the electromagnetic wave in a lossy dispersive magnetoelectric medium *J. Mod. Opt.* **62** 1323–35
- [76] Mansuripur M 2013 The force law of classical electrodynamics: Lorentz versus Einstein and Laub *Proc. SPIE* **8810** K1–18
- [77] Laue M V 1950 Zur Minkowskischen Elektrodynamik der bewegten Körper *Z. Phys.* **128**
- [78] Kinsler P, Favaro A and McCall M W 2009 Four Poynting theorems *Eur. J. Phys.* **30** 983–93
- [79] Mulser P 1985 Radiation pressure on macroscopic bodies *J. Opt. Soc. Am. B* **2** 1814–29
- [80] Mansuripur M 2012 Trouble with the Lorentz law of force: incompatibility with special relativity and momentum conservation *Phys. Rev. Lett.* **108** 193901
- [81] Tafove A 1995 *Computational Electrodynamics: the Finite-Difference Time-Domain Method* (Boston: Artech House)
- [82] Loudon R 2002 Theory of the radiation pressure on dielectric surfaces *J. Mod. Opt.* **49** 821–38
- [83] Zakharian A R, Mansuripur M and Moloney J V 2005 Radiation pressure and the distribution of electromagnetic force in dielectric media *Opt. Express* **13** 2321–36
- [84] Barnett S M and Loudon R 2006 On the electromagnetic force on a dielectric medium *J. Phys. B* **39** S671–84
- [85] Loudon R and Barnett S M 2006 Theory of the radiation pressure on dielectric slabs, prisms and single surfaces *Opt. Express* **14** 11855–69
- [86] Mansuripur M and Zakharian A R 2009 Maxwell's macroscopic equations, the energy-momentum postulates, and the Lorentz law of force *Phys. Rev. E* **79** 026608
- [87] Hinrose A 2010 Radiation pressure on a dielectric surface *Can. J. Phys.* **88** 247–52
- [88] Chau K J and Lezec H J 2011 Revisiting the Balazs thought experiment in the presence of loss: electromagnetic-pulse-induced displacement of a positive-index slab having arbitrary complex permittivity and permeability *Appl. Phys. A* **105** 267–81
- [89] Rohrbach A and Stelzer E H K 2001 Optical trapping of dielectric particles in arbitrary fields *J. Opt. Soc. Am. A* **18** 839–53

- [90] Astrath N G C, Malacarne L C, Baesso M L, Lukasievicz G V B and Bialkowski S E 2014 Unravelling the effects of radiation forces in water *Nat. Commun.* **5** 023826
- [91] Tryggvason G, Bunner B, Esmaeeli A, Juric D, Al-Rawahi N, Tauber W, Han J, Nas S and Jan Y-J A 2001 front-tracking method for the computations of multiphase flow *J. Comput. Phys.* **169** 708–59
- [92] Tryggvason G, Scardovelli R and Zaleski S 2011 *Direct Numerical Simulations of Gas–Liquid Multiphase Flows* (Cambridge: Cambridge University Press)
- [93] Balazs N L 1954 On the propagation of energy in elastic media *Proc. Phys. Soc. A* **67** 726–7
- [94] Györgyi G 1955 Die Bewegung Des Energiedimpelpunktes und der energie-impuls-tensor des elektromagnetischen *Acta. Phys.* **4** 121–31
- [95] Padgett M J 2008 On diffraction within a dielectric medium as an example of the Minkowski formulation of optical momentum *Opt. Express* **16** 20864–8
- [96] Mansuripur M 2010 Resolution of the Abraham–Minkowski controversy *Opt. Commun.* **283** 1997–2005
- [97] Ramos T, Rubilar G R and Obukhov Y N 2011 Relativistic analysis of the dielectric Einstein box: Abraham, Minkowski and total energy momentum tensors *Phys. Lett. A* **375** 1703–9
- [98] Mansuripur M 2011 Nature of electric and magnetic dipoles gleaned from the Poynting theorem and the Lorentz force law of classical electrodynamics *Opt. Commun.* **284** 594–602
- [99] Brevik I and Ellingsen S Å 2012 Detection of the Abraham force with a succession of short optical pulses *Phys. Rev. A* **86** 025801
- [100] Bell M and Green S E 1933 On radiometer action and the pressure of radiation *Proc. Phys. Soc.* **45** 320–57
- [101] Mansuripur M 2007 Radiation pressure on submerged mirrors: implications for the momentum of light in dielectric media *Opt. Express* **15** 2677–82
- [102] Mansuripur M 2012 Deducing radiation pressure on a submerged mirror from the doppler shift *Phys. Rev. A* **85** 023807
- [103] Webb K J 2013 Dependence of the radiation pressure on the background refractive index *Phys. Rev. Lett.* **111** 043602
- [104] Sheppard C J and Kemp B A 2014 Optical pressure deduced from energy relations within relativistic formulations of electrodynamics *Phys. Rev. A* **89** 013825
- [105] Palik E and Ghosh G 1998 *Handbook on Optical Constants of Solids* (San Diego: Academic)
- [106] Johnson P B and Christy R W 1972 Optical constants of the noble metals *Phys. Rev. B* **4** 4370–9
- [107] Kemp B A 2015 Macroscopic theory of optical momentum *Prog. Opt.* **60** 437–88
- [108] Loudon R 2004 Radiation pressure and momentum in dielectrics *Fortschr. Phys.* **52** 1134–40
- [109] Aanensen N S, Ellingsen S Å and Brevik I 2013 Theoretical considerations of laser-induced liquid–liquid interface deformation *Phys. Scr.* **87** 055402
- [110] Rohrbach A 2005 Stiffness of optical traps: quantitative agreement between experiment and electromagnetic theory *Phys. Rev. Lett.* **95** 168102
- [111] Barton J P, Alexander D R and Schaub S A 1989 Theoretical determination of net radiation force and torque for a spherical particle illuminated by a focused laser beam *J. Appl. Phys.* **66** 4594–602
- [112] Kajorndejnukul V, Ding W, Sukhov S, Qiu C-W and Dogariu A 2013 Linear momentum increase and negative optical forces at dielectric interface *Nat. Photonics* **7** 787–90
- [113] Ashkin A 1970 Acceleration and trapping of particles by radiation pressure *Phys. Rev. Lett.* **24** 156–9
- [114] Ashkin A, Dziedzic J M, Bjorkholm J E and Chu S 1986 Observation of a single-beam gradient force optical trap for dielectric particles *Opt. Lett.* **11** 288–90
- [115] Ashkin A 1980 Applications of laser radiation pressure *Science* **210** 1081–8
- [116] Grier D G 2003 A revolution in optical manipulation *Nature* **424** 810–6
- [117] Ashkin A 1992 Forces of a single-beam gradient laser trap on a dielectric sphere in the ray optics regime *Biophys. J.* **61** 569–82
- [118] Wright W H, Sonek G J and Berns M W 1993 Radiation trapping forces on microspheres with optical tweezers *Appl. Phys. Lett.* **63** 715–7
- [119] Wright W H, Sonek G J and Berns M W 1994 Parametric study of the forces on microspheres held by optical tweezers *Appl. Opt.* **33** 1735–48
- [120] Pfeifer R N C, Nieminen T A, Heckenberg N R and Rubinsztein-Dunlop H 2011 Optical tweezers and paradoxes in electromagnetism *J. Opt.* **13** 044017
- [121] Marston P L 2006 Axial radiation force of a Bessel beam on a sphere and direction reversal of the force *J. Acoust. Soc. Am.* **120** 3518
- [122] Sukhov S and Dogariu A 2010 On the concept of ‘tractor beams’ *Opt. Lett.* **35** 3847–9
- [123] Sukhov S and Dogariu A 2011 Negative nonconservative forces: optical ‘tractor beams’ for arbitrary objects *Phys. Rev. Lett.* **107** 203602
- [124] Novitsky A, Qiu C-W and Wang H 2011 Single gradientless light beam drags particles as tractor beams *Phys. Rev. Lett.* **107** 203601
- [125] Chen J, Ng J, Lin Z and Chan C T 2011 Optical pulling force *Nat. Photonics* **5** 531–4
- [126] Ruffner D B and Grier D G 2012 Optical conveyors: a class of active tractor beams *Phys. Rev. Lett.* **109** 163903
- [127] Brzobohatý O, Karásek V, Šíler M, Chvátal L, Čížmár T and Zemánek P 2013 Experimental demonstration of optical transport, sorting and self-arrangement using a ‘tractor beam’ *Nat. Photonics* **7** 123–7
- [128] Lee S-H, Roichman Y and Grier D G 2010 Optical solenoid beams *Opt. Express* **18** 6988–93
- [129] Leonhardt U 2014 Abraham and Minkowski momenta in the optically induced motion of fluids *Phys. Rev. A* **90** 033801
- [130] James R P A 1968 A ‘Simplest Case’ experiment resolving the Abraham–Minkowski controversy on electromagnetic momentum in matter *Proc. Natl Acad. Sci.* **68** 1149–50
- [131] Walker G B and Lahoz D G 1975 Experimental observation of Abraham force in a dielectric *Nature* **253** 339–40
- [132] Walker G B and Walker G 1976 Mechanical forces of electromagnetic origin *Nature* **263** 401
- [133] Rikken G L J A and van Tiggelen B A 2012 Observation of the intrinsic Abraham force in time-varying magnetic and electric fields *Phys. Rev. Lett.* **108** 230402
- [134] Kemp B A, Kong J A and Grzegorczyk T M 2007 Reversal of wave momentum in isotropic left-handed media *Phys. Rev. A* **75** 053810
- [135] He Y, Shen J and He S 2011 Consistent formalism for the momentum of electromagnetic waves in lossless dispersive metamaterials and the conservation of momentum *Prog. Electromagn. Res.* **116** 81–106
- [136] Mansuripur M and Zakharian A R 2012 Radiation pressure and photon momentum in negative-index media *Proc. SPIE* **8455** 845511
- [137] Casner A 2002 Déformations, manipulations et instabilités d’interfaces liquides induites par la pression de radiation d’une onde laser *PhD Thesis* University of Bordeaux